CHALMERS
UNIVERSITY OF TECHNOLOGY

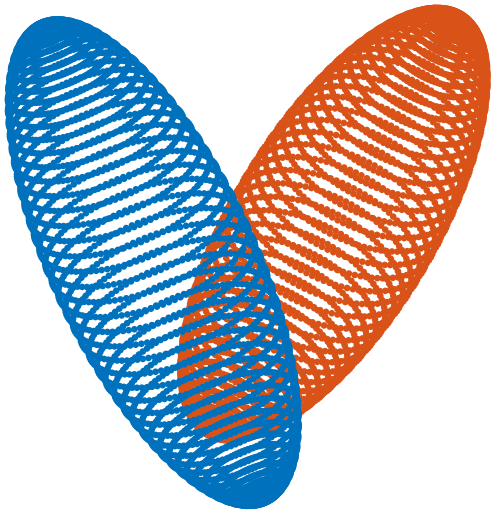

Collision rate of spheroids in turbulence

Master's thesis in Master Programme Complex Adaptive Systems

BARBARA SCHNITZER

Department of Physics
CHALMERS UNIVERSITY OF TECHNOLOGY AND GOTHENBURG UNIVERSITY
Gothenburg, Sweden 2017

Master's thesis 2017

Collision rate of spheroids in turbulence

Barbara Schnitzer

CHALMERS
UNIVERSITY OF TECHNOLOGY

Department of Physics
Statistical Physics of Complex Systems
Chalmers University of Technology and Gothenburg University
Gothenburg, Sweden 2017

Collision rate of spheroids in turbulence SCHNITZER BARBARA

Supervisor: Kristian Gustavsson and Bernhard Mehlig
Examiner: Bernhard Mehlig
Student opponent: Gustavo Stolf Jeuken

Master's thesis 2017
Department of Physics
Statistical Physics of Complex Systems
Chalmers University of Technology and Gothenburg University
SE-412 96 Gothenburg
Telephone +46 31 772 1000

Cover: Two colliding rods.

Typeset in LaTeX
Gothenburg, Sweden 2017

Collision rate of spheroids in turbulence
SCHNITZER BARBARA
Department of Physics
Chalmers University of Technology and Gothenburg University

Abstract

Collisions of particles are of great importance in different processes in fluid flows, like water droplets colliding in cumulus clouds forming rain, but also dust grains that eventually form a planet. As a continuation of work that was done on spherical particles I studied the collision rate of small spheroids in three qualitatively different flows, namely in the kinetic limit, where particles move ballistically, in the shear flow, where particles move uniformly, but can overtake each other, and in a smooth random flow, which is a model for the small scales in turbulence. A corresponding theoretical model that describes the two-dimensional collision rate was presented and compared to simulation results. It was found that the particle shape has a great influence on the collision rate in all cases. In general an increasing elongation leads to a higher collision rate, while the two-dimensional shear flow was found to be an exception in the sense that the collision rate approaches zero instead. Three-dimensional systems were investigated by simulations but not supported by a theory.

Keywords: fluid dynamics, random flow, shear flow, spheroids, collisions.

Acknowledgements

Very special thanks to my supervisor Kristian, who helped and supported me a lot throughout the work by guiding me, sharing his knowledge and discussing with me. Moreover I want to thank Bernhard, the rest of the group and the third floor of Soliden for welcoming and integrating me.
Thanks to my family and friends who always backed me up in all kinds of ways, with special thanks to Gus and Jonas for proof reading and commenting on the thesis, which improved it significantly.

Schnitzer Barbara, Gothenburg, June 2017

Contents

1
Introduction

How does rain form in clouds? How do dust grains become a planet? What are the preconditions that certain chemical reactions happen? But also how do microorganisms like plankton eat or mate in the ocean?
At first glance these questions seem mostly unrelated to each other, but having a closer look they have indeed something in common. The underlying microscopic processes are in all cases based on particles moving and colliding in a fluid flow, by what they become bigger and can form macroscopic structures. So in order to give an answer it is necessary to study how particles behave when they are subjected to a flow, what mechanisms make them approach each other and finally collide, and moreover how often they do that.

There has been done a lot of research on many similar questions aiming to understand the problem, for instance in [18, 1, 11]. However, many aspects remain not understood. In the case of organisms in water streams in the ocean [16, 9], rain formation in cumulus clouds [20, 3, 8] or even the coalescence of dust particles in accretion disks around stars in the early stages of planet formation [29, 2] it is believed that the underlying fluid is turbulent on the small scale. Turbulence is extremely hard to deal with, but there have been developed statistical models [12] that make it possible to nevertheless investigate it further, which will also be part of this thesis.

Factors that influence the collision rate can, for example, be the spatial and temporal distribution of positions determined by the flow. Under given circumstances particles might cluster together after some time, but they might also stay uniformly distributed. Furthermore the actual collision process and what happens afterwards, e.g. scattering or coalescence processes or chemical reactions, is a crucial aspect.
In addition the shape of the particles has an essential impact. So far particles are often assumed to be spherical [10, 11], which is in many cases a very good approximation, but sometimes it is very idealistic. A simplest example of a non-spherical particle is obtained by ellipses of revolution, so called 'spheroids'. Spheroids are still a caricature of real molecules but studying them provides the possibility to apply the theories to a much wider range of problems, which one has to pay with more complicated algorithms and equations.

The goal of my work is to investigate and provide basic tools to find an expression for the collision rate of small spheroids in fluid flows depending on the particles' shape as a continuation of work that has been done on spherical particles. The important difference to spherical particles is that the rotational velocity is an additional factor that has to be included in the calculations. Even though such particles have

been studied before [6, 7, 13], in particular their equations of motions and angle distributions, the collision rate has not yet been investigated.
The focus of my research lies on the collisions of advected particles, which corresponds to the very early stage of the previously given examples, where the particles are still very small such that their velocities can be approximated by the flow velocities. As soon as they become heavier advection is not an appropriate description anymore, because particles might belong to another size class or species and inertial effects will become more and more significant. Investigating such systems is another interesting research field, although it is not of importance here.

After this introduction I give a short overview of the terminology and basic concepts within fluid dynamics in chapter 2. This should provide all necessary background in order to understand the physics of the work. In chapter 3 I present previous work that has been done on the collision rate of spherical particles with respect to two particular examples, the shear flow and the random flow, which are taken up again later but for spheroids. Chapter 4 is providing all the technical details about how spheroids move and rotate in a fluid. The key words here are the Jeffery equations. In addition, two approaches how collisions between such particles can be detected are discussed and using that it is proposed a model how the analytical equation has to be modified when dealing with spheroids instead of spherical particles.
In chapter 5-7 results for three different flows are presented. At first particles in the kinetic limit with a constant velocity were investigated, followed by advected particles in the shear flow and last but not least advected particles in the random flow. The latter is very much related to appendix A, which provides a description of the statistical model of turbulence that was used.

In the thesis I look at the problem from two different perspectives. On the one hand the collision rates were extracted from simulations that were built up from scratch. On the other hand I tried to approach the problem from a more theoretical point of view starting from a basic definition of a collision. In the end the goal was to support the theory with simulations. However, not in all cases a theory was found, especially in three dimensions, but then the simulations still provide an idea of how the shape of the spheroid influences the collision rate.

To round everything off I conclude in chapter 8 and give some ideas for the continuation of this project.

2

Prerequisites

This chapter is going to provide an overview of the terminology and basic concepts underlying all the simulations and calculations contained in the thesis. It is supposed to give a reader with a different background the chance to catch up. The aim is not to overwhelm with mathematical details, it is rather to create an appropriate framework.
The compilation is based on different publications on elementary fluid dynamics [5, 24, 15, 23, 6, 10].

The first question one might ask is, what is a fluid flow and how must it be characterized? It is defined as a liquid or a gas in motion consisting of interacting particles that move around in space. Consequently the fluid has a velocity field $\mathbf{u}(\mathbf{r}, t)$, where $\mathbf{r}$ is the position of a fluid element, which consists of many individual particles with average velocity $\mathbf{u}$. The fluid element is basically a volume element around the point $\mathbf{r}$ which has certain properties. It is not straight forward why this is a correct description. It is justified by the Continuum Hypothesis [15] assuming that the size of the element is small enough compared to the whole system but at the same time big enough so that it contains sufficiently many particles in order to define a reasonable average.

The velocity gradient $\mathbb{A}(\mathbf{r}, t)$ is the Jacobi matrix of $\mathbf{u}$ and describes how the velocities change in time and space. Usually it is divided into a symmetric and an antisymmetric part, $\mathbb{S}$ and $\mathbb{O}$, as they correspond to different interpretations. The symmetric part is responsible for the shearing and deformation whereas the antisymmetric part gives rise to rotations of the individual fluid elements.

$$\mathbb{A}(\mathbf{r}, t) = \nabla \mathbf{u}^T(\mathbf{r}, t) = \underbrace{\frac{1}{2}(\mathbb{A}(\mathbf{r}, t) + \mathbb{A}^T(\mathbf{r}, t))}_{\equiv \mathbb{S}(\mathbf{r}, t)} + \underbrace{\frac{1}{2}(\mathbb{A}(\mathbf{r}, t) - \mathbb{A}^T(\mathbf{r}, t))}_{\equiv \mathbb{O}(\mathbf{r}, t)}$$

Looking at small time scales the changes of the velocity field are usually considered to be small.

The density ρ defines how many particles are in a given test volume of the flow. In many cases it is assumed that the density is constant. This does not mean that the particles always stay inside this volume but that as soon as particles leave the volume other particles have to enter it. In mathematical terms this means that the divergence of the velocity field vanishes, which is directly connected to the fluid gradients:

$$\nabla \cdot \mathbf{u}(\mathbf{r}, t) = Tr(\mathbb{A}(\mathbf{r}, t)) = 0. \tag{2.1}$$

Such a flow is called atmospheric or incompressible.
Incompressibility is often a realistic assumption and throughout my work I only deal with those kinds of fluids.

Evolving in time fluid elements are constantly subject to forces that act from all sides and that result in deformations.
In general it is the stress tensor $\mathbb{o}(\mathbf{r}, t)$ that defines the force per unit area on the fluid element. One distinguishes between normal stresses, that describe the forces that act perpendicular on the surface and that are in direct relationship to the pressure p, and shear stresses, that define the forces in other directions and that are connected to the symmetric part of the fluid gradients, as seen before.
If the flow is incompressible the deformations are volume preserving. And moreover the fluid is a so-called Newtonian fluid if the stress tensor is linearly dependent on the dynamic viscosity μ and the pressure in the following way:

$$\mathbb{o}(\mathbf{r}, t) = -p(\mathbf{r}, t)\mathbb{1} + 2\mu\mathbb{S}(\mathbf{r}, t).$$

In general, the (vector) velocity and the (scalar) pressure field can be calculated at any time using the Navier-Stokes equations. In an incompressible Newtonian fluid flow they can be derived from Newton's second law of motion $\mathbf{F} = m\mathbf{a}$ (derivation in [15]) which results in

$$\rho\left[\frac{\partial}{\partial t}\mathbf{u}(\mathbf{r}, t) + \mathbf{u}(\mathbf{r}, t) \cdot \nabla\mathbf{u}(\mathbf{r}, t))\right] = -\nabla p(\mathbf{r}, t) + \mu\nabla^2\mathbf{u}(\mathbf{r}, t) + \mathbf{f} = \nabla\mathbb{o}(\mathbf{r}, t) + \mathbf{f}.$$

The equation also takes into account external forces $\mathbf{f}$, e.g. gravitational forces, which are however neglected in my work fo reasons of simplicity.

In principle it is a huge success to have an equation that describes something non-trivial like a fluid, but there is a drawback: it is extremely hard to solve as it is a non-linear equation. It has to be treated numerically and even then it is mostly not possible with today's computer power. For that reason it has become very successful to use statistical models instead. Especially in turbulent flows those models are quite useful which is why all calculations and simulations in this thesis are dealing with those principles instead of solving Navier-Stokes. From many points of view they represent real turbulence both qualitatively and even quantitatively in an accurate way [12] even though it is basically only an idealised caricature of the real world, which of course includes special situations or regimes where it is not a sufficiently good model.

But what indicates turbulence? Very primitively it is something that looks chaotic and not ordered or uniform, nevertheless there are smaller structures like vortices or shears. Turbulence is in general very sensitive to the initial conditions.
As those are vague statements one uses dimensionless parameters in order to quantify the nature of turbulence. The concept of these parameters takes an important role in fluid dynamics. Often it does not help at all to have information about a certain variable because in order to make any statement one needs to set it into relation to a scale. For instance, from a microscopic point of view a particle in a fluid might be big, but compared to the whole system it is very tiny.

The Reynolds number Re of a fluid is such a dimensionless variable linking the characteristic time t_f of the flow to adapt to external disturbances to the time t_0 the fluid needs to travel one characteristic length scale l of the system, which could be a certain particle size or even the diameter of a pipe depending on the problem. In other words it connects the viscous and the inertia forces.

$$\mathrm{Re} = \frac{\mathrm{t_f}}{\mathrm{t_0}} = \frac{\frac{\rho \mathrm{l}^2}{\mu}}{\frac{\mathrm{l}}{\mathrm{u_0}}} = \frac{\mathrm{l u_0}}{\nu}$$

$u_0 = \dfrac{l}{t_0}$ is the characteristic flow speed and $\nu = \dfrac{\mu}{\rho}$ the kinematic viscosity which connects the dynamic viscosity and the density.
A laminar flow is created if Re is small. Here the viscous forces dominate. This means that disturbances do not have the chance to survive in a long time (on the characteristic time scale), because the fluid is able to damp the perturbations out before the fluid element has moved on the characteristic length scale, i.e. $t_0 \gg t_f$. What results is a smooth and linear flow. A very easy and but nevertheless fundamental example for a laminar flow is the shear flow. 2.1 illustrates it in two dimensions. Further discussions are in chapter 3 and 6.

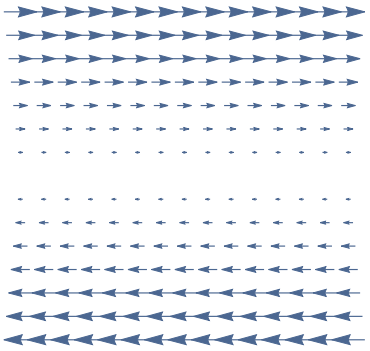

Figure 2.1: Shear flow

Increasing Re the flow becomes more turbulent, i.e. the inertial forces dominate over viscous forces, meaning that disturbances affect the fluid considerably. This is because the time it takes to 'correct' disturbances is too long compared to the characteristic time scale. A high viscosity limits the fluid to react as it has high inertia, i.e. $t_f \gg t_0$. Consequently eddies are created.

Another important dimensionless parameter that is also related to turbulence is the Kubo number Ku. It is defined a

$$\mathrm{Ku} = \frac{\mathrm{u_0}\tau}{\eta}.$$

It relates the characteristic flow speed u_0 to the speed $\frac{\eta}{\tau}$ where τ and η, called correlation time and length, characterize the small scales of the flow. The correlation length indicates the size of the smallest eddies in the turbulence, the correlation time on the other hand stands for the lifetime of these eddies. $\frac{\eta}{\tau}$ then describes the velocity of the flow fluctuations.
Therefore Ku is a measure how fast the fluid velocities fluctuate compared to the typical flow speed. $\mathrm{Ku} = 1$ is a fully developed turbulence which corresponds to a real physical turbulence. If $\mathrm{Ku} < 1$ then the the fluctuations are much faster than the flow speed, thus the flow can be considered slow. In contrast if $\mathrm{Ku} > 1$ the flow is fast as the fluctuations are considerably small.

A subsequent question that arises after having defined a fluid flow is what happens with a particle that moves in the flow. It is influenced by the flow but at the same time it also changes the flow creating perturbations, which then may affect

the particle again. Consequently the whole history of the fluid flow and the particle movement influences the situation at every time makes the whole problem extremely complicated. Therefore it is necessary to make more simplifying assumptions or investigate certain limits.

Considering a test particle in the fluid it is assigned a Stokes number St. It is another dimensionless parameter that is given by the quotient of the characteristic time of the particle to adapt to the flow t_p and the characteristic time of the fluid to change on small scales τ as defined before. It thus relates to inertia effects.

$$\mathrm{St} = \frac{\mathrm{t_p}}{\tau}$$

If St is very high particles will detach and consequently not feel the flow. In this case the fluid adapts much faster than the particle is able to. If in contrast the particle adapts much faster than the fluid changes ($\mathrm{St} \ll 1$), the particle is advected by the flow. Usually this is referred to the particle being small.
And if the particle is sufficiently small the history as well as the influences of the particle to the flow can be neglected. It simply follows the flow's streamlines, i.e. its velocity can be approximated by the fluid velocity:

$$\dot{\mathbf{r}_n} = \mathbf{u}(\mathbf{r}_n, t).$$

Advected particles are much more convenient to deal with than inertial particles and even in my work I only look at the limit of vanishing or infinite St number.

How particles actually move in the flow additionally depends on their shape. A spherical particle is completely symmetric in all directions and it is defined only by its radius r. Symmetries are always an important aspect which simplify given problems tremendously. A spherical particle can be rotated in any way but it will still look the same and behave in the same way. But as soon as symmetries are lost rotations indeed play an important role and the whole set up becomes more complicated.
The species that is dealt with in this thesis are spheroids. They are still rotationally symmetric, however only in one direction $\mathbf{n}$. This is classified as axisymmetric. The radius is exchanged with a semi axis b, being the characteristic length along $\mathbf{n}$, and another semi axis a , being the characteristic length in the two perpendicular axes to it. The aspect ratio is defined as $\lambda = \frac{b}{a}$. There are three qualitatively different shapes that come out of this.
If $\lambda < 1$ the spheroid's form is like a disk (oblate) and if $\lambda > 1$ it is rod-like (prolate). An UFO (unknown flying object) would correspond to the first case, whereas an egg, for instance, would rather be an example of the latter case. The very special case $\lambda = 1 \Leftrightarrow b = a$ reflects a spherical particle.
In two dimensions $\lambda \geq 1$. There exists a circle (=) or an ellipse (>).

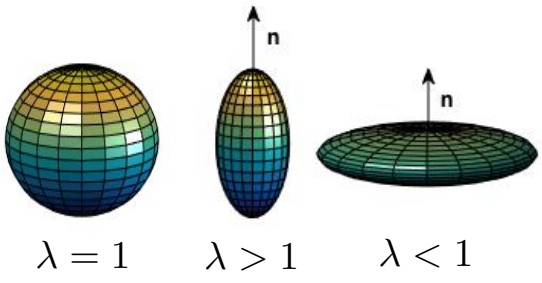

Figure 2.2: Sphere, prolate and oblate spheroid

An even further generalization would be an ellipsoid where there is no rotational symmetry anymore, thus there are three instead of two axes, but those particles are not considered here.

To summarize, this chapter gave an introduction to elementary fluid dynamics. It introduced physical quantities of a fluid flow, e.g. the velocity field and its gradients, the density and the Navier-Stokes equations. Different types of fluids like laminar, shear and turbulent flows were presented. Also the concept of dimensionless parameters was outlined as it gives rise to important features of the flow. Here the key words are the Reynolds, the Kubo and the Stokes number. The latter is important when dealing with particles moving in the flow, whereas the other two are mainly properties of the flow. Last but not least spheroids, which will be the investigated objects, were introduced.
Next I present previous work that has been done on collision rates of spherical particles in different flows before I try to generalize those concepts to spheroids.

3

Previous work - Collision rate of advected spherical particles

In order to understand how spheroids behave in a flow it is a good start to investigate advected spherical particles. There has been done a lot of work on this subject, for instance from Smoluchowski in 1917 [21], Saffman and Turner in 1956 [18] or Abrahamson in 1975 [1]. They looked at advected particles in laminar or turbulent fluid flows and found an analytical expression for the collision rate of those particles. Recently this work was further improved by Gustavsson et al. [10], who showed that the Saffman-Turner expression is just an upper bound to the actual collision rate in the case of time dependent turbulent flows. However, dealing with constant flows, like the shear flow, the expressions are still exact. In this chapter I want to sketch the approach that was used by [18, 10] and present the resulting expressions for the collision rates for two particular examples, namely the shear flow and the random flow.

3.1 Theory

In the model used the only aspect that is of interest is how often particles in the flow meet each other. Whatever happens after the actual collision, i.e. scattering or coalescence processes, is not taken into account. The reason for this assumption is that in a typical realistic system the density of colliding particles is considered low. Another way of justifying that assumption is to see the collision as a merging process of two particles. Afterwards they belong to another species or size class and they are not of interest anymore.
Computationally there are different approaches to deal with this. In [10] particles were removed which leads to a drop of the collision rate. The number density can be kept constant by adding new particles again, which might give better statistics in the end compared to the way I handled the situation, keeping all particles and let them move through each other. Particles that overlap are not allowed to collide with each other again, only as soon as they separated again. But of course, what is the better or worse solution depends very much on the specific problem that is looked at.
No matter which method is used simulations with high particle numbers densities can still be done in order to get better statistics. An alternative but inconvenient way would be to actually use a low number density and make very long simulations instead. If particles do not influence each other both ways are equivalently describing

the model.

Under the circumstances outlined above two particles with radius a collide if their relative distance becomes smaller than $2a$. This implies that their relative velocity in the normal direction $\Delta v_\xi = (\mathbf{v}_2 - \mathbf{v}_1)_\xi$ is negative while touching. They approach each other. For spherical particles the normal direction at the contact point is always the same as the relative position $\mathbf{r} = \mathbf{r}_2 - \mathbf{r}_1 = 2a\hat{\boldsymbol{\xi}}$, and thus $\Delta v_\xi = \Delta v_r$. The hat indicates that the vector is normalized and by convention pointing in the same direction as $\mathbf{r}$.

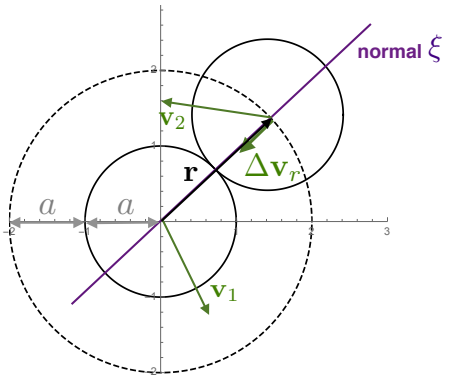

Figure 3.1: Exemplary schematic view of two colliding spherical particles.

As will be seen later for elliptical particles the direction $\hat{\boldsymbol{\xi}}$ may differ from $\mathbf{r}$ and moreover the velocity will also be influenced by the angular movement, which makes the calculation less straight forward.
Nevertheless for small spherical particles (small Stokes number) in a flow that is characterized by a velocity field $\mathbf{u}(\mathbf{r}, t)$ and a rate of strain matrix $\mathbb{A}(\mathbf{r}, t)$, as introduced in chapter 2, it is possible to approximate the relative velocity using $\mathbf{v} = \mathbf{u}(\mathbf{r}, t) \approx \mathbb{A}\mathbf{r}$ assuming that $\mathbf{u}(\mathbf{r}, t)$ varies only little for small particle separations $|\mathbf{r}| \ll \eta$.

$$\begin{aligned}\Delta v_r = \Delta v_\xi &= \hat{\boldsymbol{\xi}}^T(\mathbf{v}_2 - \mathbf{v}_1) = \hat{\boldsymbol{\xi}}^T\mathbb{A}(\mathbf{r}_2 - \mathbf{r}_1) \\ &= 2a\,\hat{\boldsymbol{\xi}}^T\mathbb{A}\hat{\boldsymbol{\xi}}\,.\end{aligned}$$

In order to take all possible collisions for a given test particle into account it is necessary to integrate over the whole surface Ω, which for the upper case corresponds to a circle (2d) or sphere (3d) with radius $2a$.

The one-particle collision rate is defined as how often a given test particles collides per time unit. For a system of spherical particles with radius a and particle number density n_0 it is equivalent to the influx through Ω:

$$\begin{aligned}\mathcal{R}_0(a, n_0) &= -n_0 \int \mathrm{d}\Omega\ \ \Delta v_\xi(2a, \Omega, t)\ \ \Theta(-\Delta v_\xi(2a, \Omega, t))\ \ \chi(2a, \Omega, t) \\ &= -2an_0 \int \mathrm{d}\Omega\ \ \hat{\boldsymbol{\xi}}^T\mathbb{A}\hat{\boldsymbol{\xi}}\ \ \Theta(-\hat{\boldsymbol{\xi}}^T\mathbb{A}\hat{\boldsymbol{\xi}})\ \ \chi(2a, \Omega, t). \qquad (3.1)\end{aligned}$$

In general the rate can be time-dependent but usually the stationary or average collision rate is considered. The Heaviside step function Θ takes care of selecting negative velocities only and the last factor, $\chi(2a, \Omega, t)$, is an indicator function which is especially important in the random flow. It is a binary function and compensates for fluctuations in time through which particles might collide more than once in a very short time. This should not influence the collision rate modelled as explained before, because the actual meeting of two particles is the essential event. Therefore χ is 1 only if the particle reaches a surface element at time t and has not previously entered it, otherwise it is 0. The indicator function is the major difference to the expression that Saffman and Turner published and makes the latter to an upper bound to the actual rate [10].

However, in an approximation where $\chi \approx 1$ and the flow is considered incompressible (constant density), which is exactly the limit that is looked at, (3.1) can be estimated in terms of the Eigenvalues of the symmetric part $\mathbb{S}$ of the strain matrix $\mathbb{A}$ according to [10]. The rotational part $\mathbb{O}$ does not contribute and can be neglected. Spherical particles do indeed rotate, but as they are considered perfectly symmetric this does not affect any collision, if and only if the particles have a small Stokes number and therefore do not significantly change the surrounding flow.
By diagonalizing the symmetric matrix $\mathbb{S}$ using an orthogonal transformation $\mathbb{T}\mathbb{S}_D\mathbb{T}^T$ the collision rate can be expressed in terms of the Eigenvalues $\sigma_1 \leq ... \leq \sigma_d$ of $\mathbb{S}$. Since $\mathbb{T}$ corresponds to a rotation and it is integrated over all directions it is also valid to drop the transformation matrices and only use $\mathbb{S}_D$:

$$\begin{aligned}\mathcal{R}_0 &= -2an_0 \int \mathrm{d}\Omega \;\; \hat{\boldsymbol{\xi}}^{\,T}\mathbb{T}\mathbb{S}_D\mathbb{T}^T\hat{\boldsymbol{\xi}} \;\; \Theta(-\,\hat{\boldsymbol{\xi}}^{\,T}\mathbb{T}\mathbb{S}_D\mathbb{T}^T\hat{\boldsymbol{\xi}}\,) \\ &\equiv -2an_0 \int \mathrm{d}\Omega \;\; \hat{\boldsymbol{\xi}}'^{\,T}\mathbb{S}_D\hat{\boldsymbol{\xi}}' \;\; \Theta(-\,\hat{\boldsymbol{\xi}}'^{\,T}\mathbb{S}_D\hat{\boldsymbol{\xi}}'\,) \\ &= -2an_0 \int \mathrm{d}\Omega \;\; \hat{\boldsymbol{\xi}}^{\,T}\mathbb{S}_D\hat{\boldsymbol{\xi}} \;\; \Theta(-\,\hat{\boldsymbol{\xi}}^{\,T}\mathbb{S}_D\hat{\boldsymbol{\xi}}\,)\;.\end{aligned}$$

In two dimensions the integral can be easily estimated using spherical coordinates $\hat{\boldsymbol{\xi}} = (\cos(u), \sin(u))^T$, and respectively $\hat{\boldsymbol{\xi}} = (\sin(v)\cos(u), \sin(v)\sin(u), \cos(v))^T$ in 3d.

$$\textbf{2d:}\quad \mathcal{R}_0 = -2an_0 \int_0^{2\pi} \mathrm{d}u\;(2a)\;\left[\sigma_1\cos(u) + \sigma_2\sin(u)\right]\;\Theta(-(\sigma_1\cos(u) + \sigma_2\sin(u)))$$

$$\begin{aligned}\textbf{3d:}\quad \mathcal{R}_0 = -2an_0 \int_0^{\pi}\int_0^{2\pi} \mathrm{d}u\,\mathrm{d}v\;(2a)^2\sin(v)\;&\left[\sigma_1\sin(v)\cos(u) + \sigma_2\sin(v)\sin(u)\right. \\ &\left.+\sigma_3\cos(v)\right]\cdot\Theta(-(\sigma_1\sin(v)\cos(u) + \sigma_2\sin(v)\sin(u) + \sigma_3\cos(v)))\end{aligned}$$

Taking into account the incompressibility (2.1), i.e. $Tr(\mathbb{A}) = Tr(\mathbb{S}) = \sum_{i=1}^{d}\sigma_i = 0$, the collision rate simplifies to

$$\begin{aligned}\textbf{2d:}\quad \mathcal{R}_0 &= -2an_0 \int_0^{2\pi} \mathrm{d}u\;(2a)\;\sigma_1\left[\cos(u) - \sin(u)\right]\;\Theta(-\sigma_1(\cos(u) - \sin(u))) \\ &= -(2a)^2 n_0\sigma_1 \int_0^{2\pi} \mathrm{d}u\;\left[\cos(u) - \sin(u)\right]\;\Theta(\cos(u) - \sin(u)) \\ &= -2(2a)^2 n_0\sigma_1 \qquad (3.2)\end{aligned}$$

$$\begin{aligned}\textbf{3d:}\quad \mathcal{R}_0 = -(2a)^3 n_0 \int_0^{\pi}\int_0^{2\pi} \mathrm{d}u\,\mathrm{d}v\;\sin(v)\;&\left[\sigma_1(\sin(v)\cos(u) - \cos(v)) + \sigma_2(\sin(v)\sin(u)\right. \\ &\left.-\cos(v)\right]\cdot\Theta(-(\sigma_1(\sin(v)\cos(u) - \cos(v)) + \sigma_2(\sin(v)\sin(u) - \cos(v))) \qquad (3.3)\end{aligned}$$

The collision rate therefore depends linearly on the number density n_0 of the system as well as quadratically/cubically on the particle radius a. The coefficient depends

on the respective flow, more specific on the Eigenvalues of the symmetric part of its strain matrix $\mathbb{A}$.
The total collision rate of the system is then given by

$$\mathcal{R} = \frac{n_0 - 1}{2}\mathcal{R}_0$$

avoiding double counting and collisions of particles with itself.

3.2 Explicit examples

In the following two special examples will be presented, the shear flow and the random flow. Later non-spherical particles in those flows are investigated, which is why this is an important starting point, not only to test the simulations but also to understand the dynamics.

3.2.1 Shear flow

The first and easier example is the shear flow (see figure 2.1). The shearing is happening in one special direction which is without loss of generality chosen to be the y-direction. In this case particles only move along the x-axis with a velocity that is determined by the y-coordinate and the shear rate s. Moreover the flow is not changing in time.

$$\mathbf{v} = \dot{\mathbf{r}} = \mathbf{u} = \begin{pmatrix} sy \\ 0 \\ 0 \end{pmatrix}, \quad \mathbb{A} = \begin{pmatrix} 0 & s & 0 \\ 0 & 0 & 0 \\ 0 & 0 & 0 \end{pmatrix}, \quad \mathbb{S} = \begin{pmatrix} 0 & \frac{s}{2} & 0 \\ \frac{s}{2} & 0 & 0 \\ 0 & 0 & 0 \end{pmatrix}.$$

The relative velocities between particles, which make them collide, only depend on the relative y-coordinate.
The Eigenvalues of the symmetric part $\mathbb{S}$ are easily calculated as there are only two non-zero elements. The collision rate can then be obtained by (3.2) and (3.3):

$$\textbf{2d:} \quad \sigma_1 = -\frac{s}{2}, \quad \sigma_2 = \frac{s}{2} \qquad \mathcal{R}_0(s, a, n_0) = 2(2a)^2 n_0 \frac{s}{2} \tag{3.4}$$

$$\textbf{3d:} \quad \sigma_1 = -\frac{s}{2}, \quad \sigma_2 = 0, \quad \sigma_3 = \frac{s}{2} \qquad \mathcal{R}_0(s, a, n_0) = \frac{4}{3}(2a)^3 n_0 s. \tag{3.5}$$

Figure 3.2 shows the result of simulating the one particle collision rate of spherical particles in a shear flow in a cubic box with length L in comparison to the previously described theoretical curve. Both coincide very well.

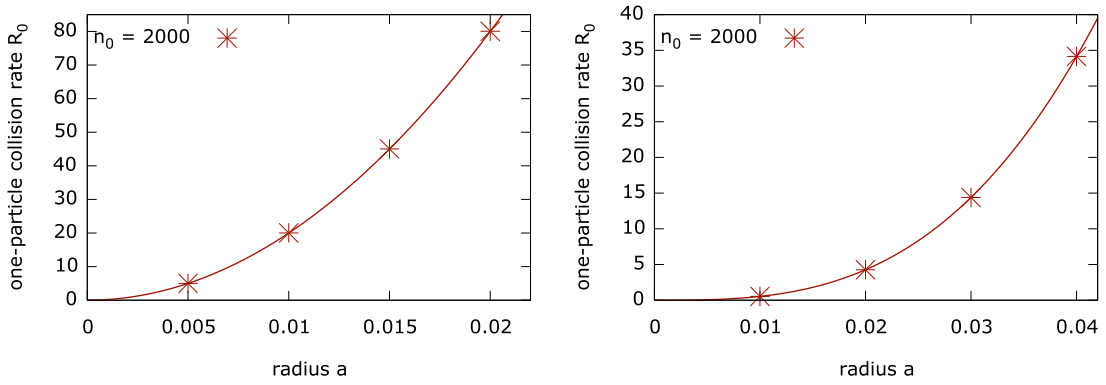

(a) **(b)**

Figure 3.2: One-particle collision rate for spherical particles with radius a in a shear flow. Uniform initialization. Markers represent the mean of 100 independent simulations. The standard error is too small to be visible. Lines show the theory. (a) 2d simulation with (3.4). (b) 3d simulation with (3.5). Parameters: $s = 25$, $n_0 = 2000$, box volume L^d with $L = 1$, $dt = 0.0005$, 10000 time steps.

3.2.2 Random flow

The next example I want to show is the collision rate in an isotropic incompressible random flow. Instead of numerically solving the Navier-Stokes equations for turbulence the flow can be modelled using a random Gaussian function $\Psi(\mathbf{r}, t)$. The fluid velocities are not only time-dependent now but also the movement is in higher than one dimension, like it was in the shear flow.

$$\Psi(\mathbf{r}, t) = (2\pi)^{d/4} \frac{\eta^{d/2+1} u_0}{\sqrt{V_d d(d-1)}} \sum_{\mathbf{k}} a_{\mathbf{k}}(t) \exp\left[\mathrm{i}\mathbf{k}\cdot\mathbf{r} - \frac{k^2\eta^2}{4}\right].$$

All details how to construct a flow from this function including the correlation function $\mathcal{C}(|\mathbf{r}-\mathbf{r}'|, |t-t'|) = \mathcal{C}(R, T) = \langle\Psi(\mathbf{r}, t)\Psi(\mathbf{r}', t')\rangle$, the flow velocity $\mathbf{u}(\mathbf{r}, t)$ and its gradient $\mathbb{A}(\mathbf{r}, t)$ are provided in Appendix A.
For the collision rate the correlation function $\mathcal{C}(R, T)$ is actually the determining ingredient. $\mathcal{R}_0$ can in principle be calculated by using (3.2 - 3.3). But it turns out to be much easier to use the general equation (3.1) as the rotational symmetry of the particles as well as some properties of the flow simplify the problem significantly.

As the first step to get a time- and space-independent collision rate the average of (3.1) is used. Moreover an isotropic flow is rotationally invariant and also the influx should be the same as the outflow, which yields to

$$\begin{aligned}\mathcal{R}_0 &= -2an_0\langle\int \mathrm{d}\Omega\ \hat{\boldsymbol{\xi}}^T\mathbb{A}\hat{\boldsymbol{\xi}}\ \Theta(-\hat{\boldsymbol{\xi}}^T\mathbb{A}\hat{\boldsymbol{\xi}})\rangle \\ &= -2an_0\cdot\left(-\frac{1}{2}\right)\langle\int \mathrm{d}\Omega\ |\hat{\boldsymbol{\xi}}^T\mathbb{A}\hat{\boldsymbol{\xi}}|\rangle. \end{aligned} \tag{3.6}$$

So instead of integrating over all u leading to a negative relative velocity component in the normal direction, it is valid to integrate over the absolute value with a factor of $-\frac{1}{2}$, which takes into account that only the influx, i.e. negative relative velocities, is important.

Additionally (3.6) is integrated over all directions, which are symmetric. Therefore it is without loss of generality equal to just use one particular direction now chosen to be in the x-direction. Furthermore by the assumption that the distance between particles $|\mathbf{r}|$ during the collision are much smaller than the correlation length η (requiring that the particle radius $a \ll \eta$, remember that η is a measure of the smallest eddies in the system) one can series expand the equation for the correlation function around $|\mathbf{r}| = R = 0$ and what remains is the term

$$\mathcal{R}_0 = an_0\langle|\mathbb{A}_{xx}(0,0)|\rangle \int \mathrm{d}\Omega = an_0\langle|\mathbb{A}_{xx}(0,0)|\rangle \cdot A_d(2a).$$

$A_d(2a)$ is the surface area of a d-dimensional sphere with radius $2a$. Especially for advected particles this turns out to be a very good approximation.

There is one more fact that can be used. As the components of $\mathbb{A}$ are Gaussian distributed random numbers, $\langle|\mathbb{A}_{xx}(0,0)|\rangle$ can be replaced by $\sqrt{\frac{2}{\pi}}\sqrt{\langle\mathbb{A}_{xx}(0,0)\mathbb{A}_{xx}(0,0)\rangle}$.

Finally the collision rate reduces to

$$\mathcal{R}_0 = \frac{n_0}{\sqrt{2\pi}} \cdot A_d(2a) \cdot 2a \cdot \sqrt{\langle\mathbb{A}_{xx}(0,0)\mathbb{A}_{xx}(0,0)\rangle} \tag{3.7}$$

and from appendix (A.3): $\langle\mathbb{A}_{xx}(0,0)\mathbb{A}_{xx}(0,0)\rangle = \dfrac{u_0^2}{d\cdot\eta^2}$.

Applied to two and three dimensions

2d: $A_2(2a) = 2\pi \cdot 2a$

$$\Rightarrow \quad \mathcal{R}_0(a, n_0, u_0, \eta) = \frac{n_0}{\sqrt{2\pi}} \cdot 2\pi \cdot 2a \cdot 2a \cdot \sqrt{\frac{u_0^2}{2\eta^2}} = 8n_0\sqrt{\pi}a^2\frac{u_0}{\eta} \tag{3.8}$$

3d: $A_3(2a) = 4\pi \cdot (2a)^2$

$$\Rightarrow \quad \mathcal{R}_0(a, n_0, u_0, \eta) = \frac{n_0}{\sqrt{2\pi}} \cdot 4\pi \cdot (2a)^2 \cdot 2a \cdot \sqrt{\frac{u_0^2}{3\eta^2}} = \frac{32}{\sqrt{6}}n_0\sqrt{\pi}a^3\frac{u_0}{\eta}. \tag{3.9}$$

Both cases can be reproduced very well by the simulations. Note that the result is indeed the Saffman-Turner expression in this case. For $\mathrm{Ku} = 0.1, 1$ the collision scheme where particles are allowed to recollide after they have been separated by $2a$ is $\chi = 1$, which is why both theories coincide.

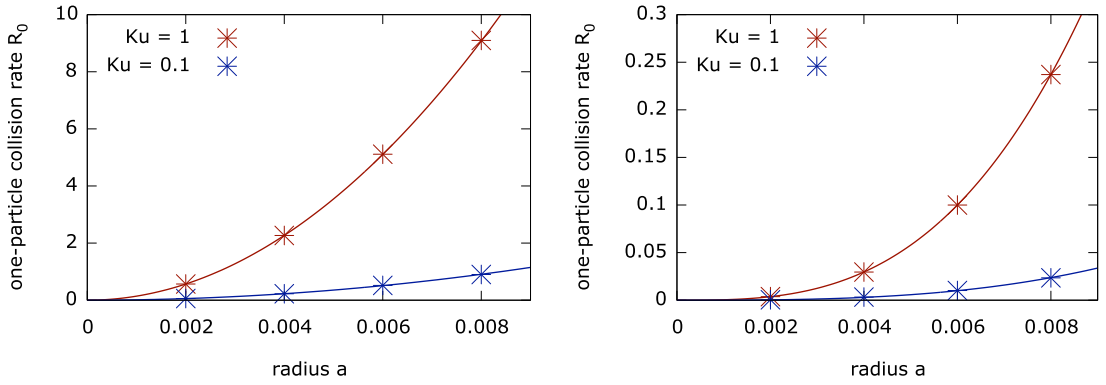

(a) **(b)**

Figure 3.3: One-particle collision rate for spherical particles with radius a in a random flow for different Ku. Uniform initialization. Markers represent the mean of 100 independent simulations. The standard error is too small to be visible. Lines show the theory. (a) 2d simulation with (3.8). (b) 3d simulation with (3.9). Simulation parameters: $n_0 = 2000$, $\eta = 0.1$, $\tau = 0.1$, box volume L^d with $L = 1$, $dt = 0.0005$, 5000 time steps.

4

Methods

The next step towards the goal of this project, to find the collision rate of spheroids in a random flow, is to build up both a set of appropriate tools for simulating the scenario and also a foundation for a theory.
Regardless of the actual collisions there must be certain mechanisms that drive the motion of spheroids in a flow and underlie the fact that they collide at all. In the early 1900s Jeffery was concerned with this problem and in 1922 he answered the question, how advected spheroids behave in fluid flows [13]. He proposed a set of equations that reflect their motion, called the Jeffery equations. Adapted to our specific problem they are outlined in the first part of this chapter.
Next an important ingredient is to investigate when two spheroids actually collide. It cannot be as trivial as for spherical particles due to less symmetry, but in the second part an algebraic condition for two spheroids to touch, which is equivalent to them colliding if additionally the relative velocity of the contact point is negative, is given. This algorithm is the basis of all simulations that were performed.
The third part is dealing with a geometric approach to find a collision condition which was later used to generalize the theoretical collision rate for spherical to axisymmetric particles making it possible to compare simulations to an analytic expression. The last part shows how to include the angular movement of the particles in the equation for the collision rate. In the last two sections it is concentrated on the two dimensional problem only.
To put it in a nutshell, this chapter is supposed to give more technical details and insight in the methods used.

4.1 Equations of motion - Jeffery's equations

The position of a spheroid in a flow is always defined by the coordinates of it centre as well as the unit vector in its rotation symmetry axis $\mathbf{n}(t)$. Using spherical coordinates $\{r, \phi, \theta\}$ it is parametrized by

$$\mathbf{n}(t) = \Big(\sin(\theta)\cos(\phi), \quad \sin(\theta)\sin(\phi), \quad \cos(\theta)\Big)^T .$$

Note that $\mathbf{n}(t)$ has to be normalized at any time, which is why the radius component can be neglected.
An advected particle has no inertia and its motion is only determined by the fluid velocity. This is actually a consequence of Stokes law in the limit of $St \to 0$. Its

translational movement through the flow is therefore easily determined by

$$\frac{\mathrm{d}\mathbf{r}(t)}{\mathrm{d}t} = \mathbf{u}(\mathbf{r}, t).$$

Now comes the more difficult part: how does $\mathbf{n}$ change? In other words, how does the orientation of the spheroid change while moving through a fluid?
To answer this question one has to investigate Jeffery's equations published in 1922 [13]. Furthermore Jonas Einarsson gave a great summary and explanation of those equations and their consequences within his Licentiate Thesis in 2013 [6]. Nevertheless the most important aspects are summarized again in the following.

The equation of motion of $\mathbf{n}(t)$ is a non-linear expression which depends on the fluid gradient $\mathbb{A} = \mathbb{S} + \mathbb{O}$ and the aspect ratio λ, as defined in chapter 2.

$$\frac{\mathrm{d}\mathbf{n}(t)}{\mathrm{d}t} = \mathbb{O}\mathbf{n}(t) + \underbrace{\frac{\lambda^2 - 1}{\lambda^2 + 1}}_{\equiv\Lambda} \left(\mathbb{S}\mathbf{n}(t) - \mathbf{n}(t)\mathbf{n}^T(t)\mathbb{S}\mathbf{n}(t)\right) \tag{4.1}$$

Here the shape parameter Λ is introduced. $\Lambda \in (-1, 1)$ and governs if the spheroid is oblate ($\Lambda < 0$) or prolate ($\Lambda > 0$). $\Lambda = 0$ corresponds to a spherical particle. Moreover in two dimensions from $\lambda \geq 1$ follows $\Lambda \geq 0$.

For a general matrix $\mathbb{A}_{ij}$ and using spherical coordinates (ϕ, θ) (4.1) is equivalent to

$$\begin{aligned}\dot{\phi} = \frac{1}{2} \Big\{ & (\mathbb{A}_{01} - \mathbb{A}_{10}) + \Lambda(\mathbb{A}_{01} + \mathbb{A}_{10})\cos(2\phi) - \Lambda(\mathbb{A}_{00} - \mathbb{A}_{11})\sin(2\phi) \\ & + \frac{\cos(\theta)\cos(\phi)}{\sin(\theta)} \cdot ((\mathbb{A}_{12} - \mathbb{A}_{21}) + \Lambda(\mathbb{A}_{12} + \mathbb{A}_{21})) \\ & - \frac{\cos(\theta)\sin(\phi)}{\sin(\theta)} \cdot ((\mathbb{A}_{02} - \mathbb{A}_{20}) + \Lambda(\mathbb{A}_{02} + \mathbb{A}_{20})) \Big\}\end{aligned} \tag{4.2}$$

$$\begin{aligned}\dot{\theta} = \frac{1}{4} \Big\{ & \Lambda\sin(2\theta) \cdot (\mathbb{A}_{00} + \mathbb{A}_{11} - 2\mathbb{A}_{22} + (\mathbb{A}_{00} - \mathbb{A}_{11})\cos(2\phi) + (\mathbb{A}_{01} + \mathbb{A}_{10})\sin\,(2\phi)) \\ & + 2\sin(\phi) \cdot ((\mathbb{A}_{12} - \mathbb{A}_{21}) + \ \Lambda(\mathbb{A}_{12} + \mathbb{A}_{21})\cos(2\theta)) \\ & + 2\cos(\phi) \cdot ((\mathbb{A}_{02} - \mathbb{A}_{20}) + \Lambda(\mathbb{A}_{02} + \ A_{20})\cos(2\theta)) \Big\}.\end{aligned} \tag{4.3}$$

As a side remark, $\sin(\theta)$ has roots for $\theta = k\pi, k \in \mathbb{Z}$, which could lead to big changes in ϕ for those particular θ according to (4.2). However, the changes are in fact not noticeable because they correspond to a rotation around the symmetry axis.
Even though (4.2 - 4.3) are non-linear the underlying motion is indeed not. It is a consequence of the normalization of $\mathbf{n}(t)$. And it can be shown that there are three regimes of possible behaviour depending on the Eigenvalues of the matrix $\mathbb{B} = \Lambda\mathbb{S} + \mathbb{O}$. Either $\mathbf{n}(t)$ is aligning with the strongest Eigendirection (largest Eigenvalue), or it spirals in to or out of this direction. The phase transitions happens at specific values.
Another interesting result is that the change from rod like particles to disk shaped ones is precisely equivalent to the change from $Tr(\mathbb{B}^3)$ to $-Tr(\mathbb{B}^3)$ (Tr is referring

to the trace of the matrix), i.e. in a flow where rods spiral in, disks would spiral out, and vice versa.

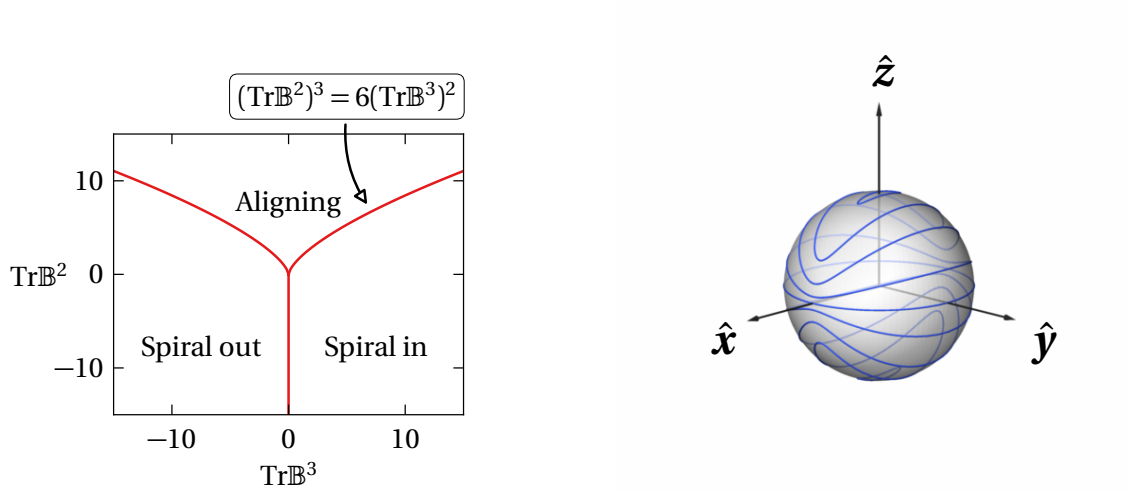

(a) Time evolution of $\mathbf{n}(t)$ with respect to the strongest Eigendirection of $\mathbb{B} = \Lambda\mathbb{S} + \mathbb{O}$

(b) Examples for paths of $\mathbf{n}(t)$ in a shear flow

Figure 4.1: source: [6]

In a simple shear flow ($\mathbb{A}$ defined as in 3.2.1) $Tr(\mathbb{B}^3) = 0$ and $Tr(\mathbb{B}^2) < 0$. It is therefore precisely on the boundary which leads neither to periodically going away nor approaching but to a stable tumbling shown in figure 4.1b. As $\mathbf{n}(t)$ is always a unit vector the trajectories conditioned on the initial state lie on a unit sphere. They are called Jeffery orbits.

All in all the movement of spheroids advected in a flow is defined by equation (4.1). It depends on their shape and the velocity gradients $\mathbb{A}$. In contrast to advected spherical particles, which only follow the streamlines and where rotations are not relevant, spheroids might also end up in a periodic movement called tumbling. Furthermore there is a connection between disks and rods with the same axis lengths.

4.2 Algebraic collision detection

Dealing with spherical particles the only condition for a collision is that the distance between their centres is smaller than the sum of their radii. In contrast, it is not that easy anymore when dealing with spheroids. The way their angles are relative to each other is an essential ingredient. Even though two ellipsoids are potentially close to each other their angular movements can cause that they nevertheless do not collide. They are able to avoid each other in an elegant manner. At the same time, particles that move away from each other can still rotate into each other.
In 2001 Wang et al. [26, 17] proposed an algorithm which gives an algebraic condition that allows to distinguish between overlapping, touching and separated ellipsoids based on their positions and tilts. The motivation of their work was however coming from a total different perspective, namely gaming industry. Objects in games are

often approximated by many connected spheroids and, in order to find out if those objects touch or if a body can move in a certain direction without colliding with others, such algorithms are needed. In 2009 they complemented their previous work [27] and applied it to the same problem that is faced in this work, the collision detection of ellipsoids. It is even more general as spheroids are special ellipsoids. It is a very powerful and computationally cheap algorithm which is moreover exact. The basic idea is illustrated in the following.

A canonical ellipsoid $\mathcal{E}^0$ is centred at the origin with semi axes a, b and c in the x-, y- and z-directions respectively and moreover $a \leq b \leq c$. Its surface is given by the equation

$$\mathcal{E}^0 : \mathbf{x}^T E \mathbf{x} = \begin{pmatrix} x & y & z & 1 \end{pmatrix} \begin{pmatrix} \frac{1}{a^2} & 0 & 0 & 0 \\ 0 & \frac{1}{b^2} & 0 & 0 \\ 0 & 0 & \frac{1}{c^2} & 0 \\ 0 & 0 & 0 & -1 \end{pmatrix} \begin{pmatrix} x \\ y \\ z \\ 1 \end{pmatrix} = 0$$

The interior of the ellipsoid is instead described by $\mathbf{x}^T E \mathbf{x} < 0$.

A general ellipsoid is however centred at x_c, y_c and z_c and additionally tilted by θ and ϕ defined precisely like the angles in spherical coordinates. In this case an affine transformation $\mathcal{M}$ consisting of a rotation $\mathcal{R}$ followed by a translation $\mathcal{T}$ has to be applied to E.

$$\begin{aligned} \mathcal{M} &= \mathcal{T}(x_c, y_c, z_c) \cdot \mathcal{R}(\theta, \phi) = \mathcal{T}(x_c, y_c, z_c) \cdot \mathcal{R}_z(\phi) \cdot \mathcal{R}_y(\theta) \\ &= \begin{pmatrix} 1 & 0 & 0 & x_c \\ 0 & 1 & 0 & y_c \\ 0 & 0 & 1 & z_c \\ 0 & 0 & 0 & 1 \end{pmatrix} \begin{pmatrix} \cos(\phi) & -\sin(\phi) & 0 & 0 \\ \sin(\phi) & \cos(\phi) & 0 & 0 \\ 0 & 0 & 1 & 0 \\ 0 & 0 & 0 & 1 \end{pmatrix} \begin{pmatrix} \cos(\theta) & 0 & \sin(\theta) & 0 \\ 0 & 1 & 0 & 0 \\ -\sin(\theta) & 0 & \cos(\theta) & 0 \\ 0 & 0 & 0 & 1 \end{pmatrix} \end{aligned}$$

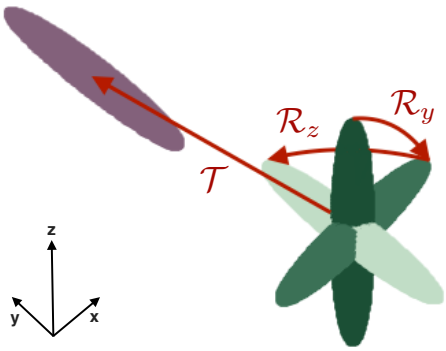

Figure 4.2: Transformation $\mathcal{M}$.

Likewise it is valid to apply $\mathcal{M}^{-1}$ to the coordinate vector $\mathbf{x}$. This leads to a more general equation for $\mathcal{E}$.

$$\mathcal{E} : \mathbf{x}^T (\mathcal{M}^{-1})^T E \mathcal{M}^{-1} \mathbf{x} \leq 0 \qquad (4.4)$$

If two ellipsoid $\mathcal{E}_1$ and $\mathcal{E}_2$, each defined by (4.4) with transformations $\mathcal{M}_{1,2}$, collide it means that they have exactly one common point, the touching point. If they overlap they share parts of their interior.
In [26] it was shown that these statements are equivalent to investigating the number of negative roots in μ of the characteristic equation

$$f(\mu) = \det \left[\mu (\mathcal{M}_1^{-1})^T E \mathcal{M}_1^{-1} - (\mathcal{M}_2^{-1})^T E \mathcal{M}_2^{-1} \right] = 0.$$

1. Two ellipsoids are separate if and only if the characteristic equation has two distinct negative roots.

2. They are touching each other if and only if the characteristic equation has a negative double root.
3. Otherwise they are overlapping.

Consequently, one has to solve a polynomial equation of order 4. However, it is not necessary to have the full knowledge about the roots. It's is sufficient to know their signs. This can easily be done by counting the sign changes of the Sturm Sequence of $f(\mu)$ between $-\infty$ and 0. In [4, p.288ff.] it is explained in detail how it works.

So, if two ellipsoids touch they have according to these rules a negative double root mu_0. The touching point $\mathbf{x}_0$ is uniquely defined and fullfills

$$(\mu_0 E - E)\mathbf{x}_0 = 0.$$

In general these principles are easily applied to spheroids by setting $a = b$ for prolate and $b = c$ for oblate spheroids. Furthermore the two-dimensional case is expressed by $a = b$ and $\theta = \frac{\pi}{2}$. After the rotation $\mathcal{R}_y(\theta = \frac{\pi}{2})$ the cut through the x-y-plane would precisely result in an ellipse with major axis c and minor axis $a = b$.

With the scheme outlined above collisions are easily checked in the simulation. It can be even further optimized by using a basic sweep-and-prune algorithm [22]. By tracking the objects in a sorted list in each direction only those that are sufficiently close to each other are checked for collision. In addition to that the insertion sort algorithm for almost sorted lists can be used in each time step because it is assumed that the positions do not change much within a small time interval.
The combination of those methods builds a powerful basis of the computational part of this work.

4.3 Geometric collision condition

The collision rate is defined as influx through a certain surface around a test particle. Going from spherical particles, where the surface is again a sphere (with radius $2a$), to spheroids the description becomes more complicated. The previously described algebraic method should in principle also define this surface. However, this turned out to be extremely hard to solve, which is why in this section another approach is presented. The calculations are shown in two dimensions for ellipses with major axis c and minor axis a where the surface corresponds to a line.
The first goal is to find an expression for the positions of the ellipses' centres (x_c, y_c) such that they touch a given canonical test ellipse, because it constitutes a necessary condition for a collision. The expressions will now be dependent on the difference of their orientations $\phi = \phi_2 - \phi_1$.
A general ellipse at point (x_c, y_c) rotated by ϕ is given by the parametrized equations

$$\begin{pmatrix} x \\ y \end{pmatrix} = \begin{pmatrix} x_c + c\cos(u)\cos(\phi) - a\sin(u)\sin(\phi) \\ y_c + c\cos(u)\sin(\phi) + a\sin(u)\cos(\phi) \end{pmatrix}$$

where $u \in [0, 2\pi)$. Moreover it is sufficient to consider the relative angle $\phi \in [0, \pi)$ due to the symmetry of the ellipse. Throughout the calculation those restrictions

are considered. However, because of the periodicity other angular ranges of length π would still give correct results.
For $\phi = 0$ and $x_c = y_c = 0$ this reduces to the canonical ellipse. If a canonical and a general ellipse touch each other this means that

$$\underbrace{\begin{pmatrix} c\cos(u) \\ a\sin(u) \end{pmatrix}}_{\text{can. ellipse}} = \underbrace{\begin{pmatrix} x_c + c\cos(\tilde{u})\cos(\phi) - a\sin(\tilde{u})\sin(\phi) \\ y_c + c\cos(\tilde{u})\sin(\phi) + a\sin(\tilde{u})\cos(\phi) \end{pmatrix}}_{\text{gen. ellipse}}.$$

The parametric angles u and $\tilde{u}$ are not necessarily the same for both bodies strongly depending on ϕ. The solution for (x_c, y_c) is then given by

$$\begin{pmatrix} x_c \\ y_c \end{pmatrix} = \begin{pmatrix} c\cos(u) - c\cos(\tilde{u})\cos(\phi) + a\sin(\tilde{u})\sin(\phi) \\ a\sin(u) - c\cos(\tilde{u})\sin(\phi) - a\sin(\tilde{u})\cos(\phi) \end{pmatrix}. \tag{4.5}$$

Now the idea is to find an expression for $\tilde{u}$ which is dependent on u resulting in the wanted parametric curves for the centres. This can be done by investigating another touching condition: if the ellipses touch their tangential angle α at the touching point has to be the same. But one has to pay attention to the fact that there are always two solutions, shown by the green lines in figure 4.3b. Think about moving the tilted ellipse counter clockwise around the other one such that they constantly touch. While doing so the relative position of the two centres $\mathbf{r}$ draws the two lines in figure 4.3a, depending on which side of the ellipse is used (dashed or solid line). Dealing with colliding rigid bodies the interesting solution is of course the outer curve.

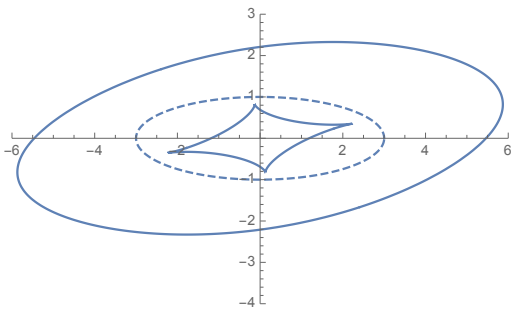

(a) Two curves for (x_c, y_c) because there are always two solutions for the same tangential angle.

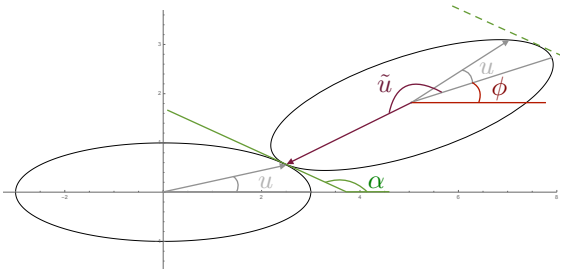

(b) Schematic view of the important angles.

Figure 4.3

The following calculation presents how to find $\tilde{u}$ and therefore get a closed form solution of (x_c, y_c). The tangential angle at u is given by

$$-\tan(u) = \frac{a}{c}\cot(\alpha).$$

For the same u the tangential angle for the tilted ellipse is

$$-\tan(u) = \frac{a}{c}\cot(\alpha + \phi) = \frac{a}{c}\frac{\cot(\alpha)\cot(\phi) - 1}{\cot(\alpha) + \cot(\phi)}. \tag{4.6}$$

The aspect ratio is defined as $\lambda = \frac{c}{a}$.

As we are looking for the angle $\tilde{u}$ which is the parametric angle where the rotated ellipse has the tangential angle α equation (4.6), is solved for $\cot(\alpha)$ resulting in

$$\frac{1}{\lambda}\cot(\alpha) = \frac{-\tan(u)\cot(\phi) + \frac{1}{\lambda}}{\cot(\phi) + \lambda\tan(u)} = \frac{\frac{1}{\lambda}\cos(u)\sin(\phi) - \sin(u)\cos(\phi)}{\cos(\phi)\cos(u) + \lambda\sin(\phi)\sin(u)} \equiv -\tan(\tilde{u})$$

$$\Leftrightarrow \quad \tilde{u} = \pi + \arctan 2\left(\sin(u)\cos(\phi) - \frac{1}{\lambda}\cos(u)\sin(\phi), \cos(\phi)\cos(u) + \lambda\sin(u)\sin(\phi)\right)$$

$$\equiv \pi + \arctan 2\left(h(u,\phi), g(u,\phi)\right). \tag{4.7}$$

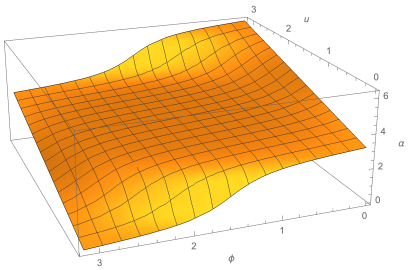

Figure 4.4: Equation (4.7) for $\lambda = 3$.

The arcus tangent 2 is defined as

$$\arctan 2(y,x) = \begin{cases} \arctan(\frac{y}{x}) & \text{if } x > 0 \\ \arctan(\frac{y}{x}) + \pi & \text{if } x < 0 \wedge y \geq 0 \\ \arctan(\frac{y}{x}) - \pi & \text{if } x < 0 \wedge y < 0 \\ \frac{\pi}{2} & \text{if } x = 0 \wedge y > 0 \\ -\frac{\pi}{2} & \text{if } x = 0 \wedge y < 0 \\ \text{undefined} & \text{if } x = 0 \wedge y = 0 \end{cases}$$

and therefore gives values between $-\pi$ and π.

Additionally it was chosen to add π in (4.7) which does not affect α but determines the correct side of the ellipse (see green lines in figure 4.3a). Finally the outer curve is chosen instead of the inner.

Inserting the result from (4.7) into the general equation for (x_c, y_c) (4.5) one gets the wanted curve using basic trigonometric identities.

$$x_c = a\left(\lambda\cos(u) + \frac{\lambda\cos(\phi)g(u,\phi) - \sin(\phi)h(u,\phi)}{\sqrt{g(u,\phi)^2 + h(u,\phi)^2}}\right) \tag{4.8}$$

$$y_c = a\left(\sin(u) + \frac{\lambda\sin(\phi)g(u,\phi) + \cos(\phi)h(u,\phi)}{\sqrt{g(u,\phi)^2 + h(u,\phi)^2}}\right) \tag{4.9}$$

The solutions are in general non-trivial and one has to be very careful with the construction of $\tilde{u}$.

Examples for the curves for different relative angles ϕ are shown in figure 4.5.

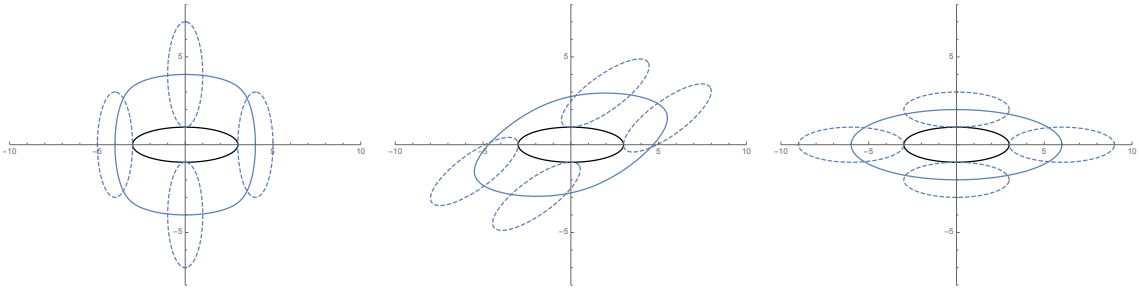

Figure 4.5: Different curves (x_c, y_c) for $\lambda = 3$. Left: $\phi = \frac{\pi}{2}$. Middle: $\phi = \frac{\pi}{4}$. Right: $\phi = 0$.

In the special case of $\phi = 0$ the curve is just an ellipse with major axis $c' = 2c$ and minor axis $a' = 2a$ because only then $\tilde{u}$ is a linear function given by $\tilde{u} = u + \pi$.

In order to get the whole circumference for each ϕ the line integral over infinitely small line segments has to be performed. In general the curves are rotationally symmetric by π and for that reason it is enough to perform the integration over u from 0 to π and double the result.

$$l = 2 \int_0^{\pi} \underbrace{\sqrt{\left[\frac{\mathrm{d}x_c}{\mathrm{d}u}\right]^2 + \left[\frac{\mathrm{d}y_c}{\mathrm{d}u}\right]^2}}_{\equiv \Delta l} \mathrm{d}u \tag{4.10}$$

Those integrals are hard to solve exactly. However, numerically one can perform the integrations for different values of ϕ. What I find is that the length of the curve l does not dependent on the value of ϕ, which corresponds to the difference of the orientation of the ellipses. This is a rather unexpected and non-intuitive result simplifying the whole problem a lot. In some cases it makes the integration for all values of ϕ redundant. Instead it is sufficient to perform the integral for one specific ϕ, e.g. the simplest case $\phi = 0$.
Mathematically the statement is expressed by

$$l = const. \quad \Leftrightarrow \quad \frac{\mathrm{d}l}{\mathrm{d}\phi} = 0. \tag{4.11}$$

As the function is continuous and differentiable within the integration boundaries it is allowed to exchange the integral and the derivative.

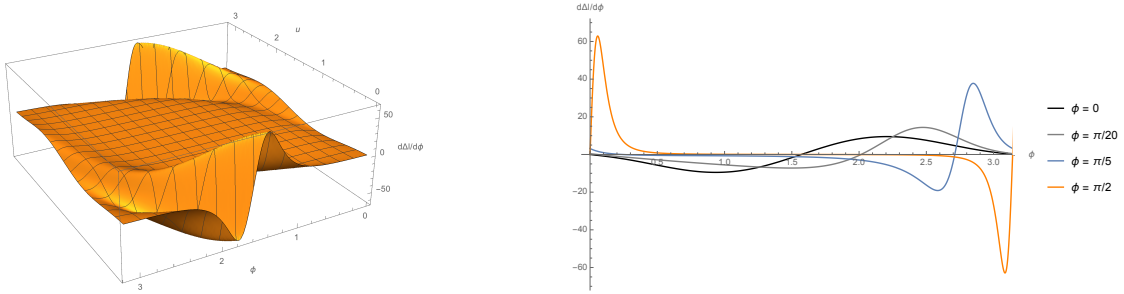

(a) **(b)**

Figure 4.6: (a) Change $\frac{\mathrm{d}\Delta l}{\mathrm{d}\phi}$ of l with respect to ϕ as a function of ϕ and u. (b) Example curves of $\frac{\mathrm{d}\Delta l}{\mathrm{d}\phi}$ for different ϕ each dependent on u

Looking at figure 4.6a the speculation would be that for every ϕ the integrand is odd which would lead to the whole integral being zero. Unfortunately it is not generally like that, as seen in figure 4.6b. Only for $\phi = 0$ and $\phi = \frac{\pi}{2}$ it is actually the case.

The derivatives of x_c and y_c with respect to u after some simplifications are

$$\begin{aligned}
\frac{\mathrm{d}x_c}{\mathrm{d}u} &= a\left(-\lambda\sin(u) + \frac{(\lambda\cos(\phi)h(u,\phi) + \sin(\phi)g(u,\phi))\cdot(h(u,\phi)\frac{\partial g(u,\phi)}{\partial u} - g(u,\phi)\frac{\partial h(u,\phi)}{\partial u})}{(g(u,\phi)^2 + h(u,\phi)^2)^{\frac{3}{2}}}\right) \\
&= a\left(-\lambda\sin(u) + \frac{\lambda\sin(u)\cdot(-1)}{(g(u,\phi)^2 + h(u,\phi)^2)^{\frac{3}{2}}}\right) \\
&= -a\lambda\sin(u)\left(1 + \frac{1}{(g(u,\phi)^2 + h(u,\phi)^2)^{\frac{3}{2}}}\right) \\
\frac{\mathrm{d}y_c}{\mathrm{d}u} &= a\left(\cos(u) + \frac{(-\cos(\phi)g(u,\phi) + \lambda\sin(\phi)h(u,\phi))\cdot(h(u,\phi)\frac{\partial g(u,\phi)}{\partial u} - g(u,\phi)\frac{\partial h(u,\phi)}{\partial u})}{(g(u,\phi)^2 + h(u,\phi)^2)^{\frac{3}{2}}}\right) \\
&= a\left(\cos(u) + \frac{-\cos(u)\cdot(-1)}{(g(u,\phi)^2 + h(u,\phi)^2)^{\frac{3}{2}}}\right) \\
&= a\cos(u)\left(1 + \frac{1}{(g(u,\phi)^2 + h(u,\phi)^2)^{\frac{3}{2}}}\right).
\end{aligned}$$

Only a factor of $(-\lambda\tan(u))$ distinguishes the two expressions. Therefore (4.11) can be further simplified.

$$\begin{aligned}
\frac{\mathrm{d}l}{\mathrm{d}\phi} &= 2\int_0^\pi \frac{\mathrm{d}}{\mathrm{d}\phi}\left(\sqrt{\left[\frac{\mathrm{d}y_c}{\mathrm{d}u}\right]^2(\lambda^2\tan^2(u)) + \left[\frac{\mathrm{d}y_c}{\mathrm{d}u}\right]^2}\right)\mathrm{d}u \\
&= 2\int_0^\pi \frac{\mathrm{d}}{\mathrm{d}\phi}\left(\sqrt{\left[\frac{\mathrm{d}y_c}{\mathrm{d}u}\right]^2(\lambda^2\tan^2(u)+1)}\right)\mathrm{d}u \\
&= 2\int_0^\pi \frac{\mathrm{d}\Delta l}{\mathrm{d}\phi}\,\mathrm{d}u \overset{!}{=} 0
\end{aligned} \tag{4.12}$$

Solving equation (4.12) is not trivial and goes beyond the scope of this work. Numerical calculations nevertheless show that (4.12) vanishes.

After all, using this statement the pure integration over the surface for every ϕ can be exchanged by a simple elliptic integral with major axis $2c$ and minor axis $2a$ corresponding to $\phi = 0$. The canonical ellipse's circumference $\mathcal{E}^0$ is defined by the

parametric curve $x_c = 2c\cos(u)$ and $y_c = 2a\sin(u)$.

$$\begin{aligned}
\int_{\mathcal{E}^0} \mathrm{d}\Omega &= \int_0^{2\pi} \mathrm{du}\ \sqrt{\left[\frac{\mathrm{d}x_c}{\mathrm{du}}\right]^2 + \left[\frac{\mathrm{d}y_c}{\mathrm{du}}\right]^2} = \int_0^{2\pi} \mathrm{du}\ \sqrt{(2c)^2\sin^2(u) + (2a)^2\cos^2(u)} \\
&= 4\int_0^{\frac{\pi}{2}} \mathrm{du}\ \sqrt{(2c)^2\sin^2(u) + (2a)^2(1-\sin^2(u))} \\
&= 4(2c)\int_0^{\frac{\pi}{2}} \mathrm{du}\ \sqrt{1 - k^2\sin^2(u)} \qquad\qquad k^2 \equiv 1 - \frac{a^2}{c^2} = 1 - \frac{1}{\lambda^2} \\
&= 4(2c)E(k^2) = 4\lambda(2a)E(k^2) = 8\lambda a E(k^2) \qquad (4.13)
\end{aligned}$$

with $E(k^2)$ being a complete elliptic integral of second kind. k is equivalent to the eccentricity of the ellipse.
The curves for (x_c, y_c) as well as the result that the lengths of the curves do not depend on the relative angle ϕ were used in order to calculate the actual collision rates for the systems investigated in the following chapters.

In three dimensions the simulations presented in chapter 5 indicate that the surface area is indeed dependent on the relative angle. The strategy to build up those integrals is equal to two dimensions. However, it becomes more complicated and would be worth another individual project. Thus, in the theoretical part of this work I concentrate on the lower dimensional case.

4.4 Collision rate including the angular velocity

So far only the situation where rotations do not matter, as for spherical particles, were discussed. In the following I want to show how to include the angular momenta of elliptical particles with minor axis a and aspect ratio λ in the theoretical model for the collision rate (see chapter 3). Also here the focus is only on two dimensions.

The most important change is that the influx is no longer only determined by the relative translational velocity $\Delta\mathbf{v}$, but also the relative velocity of the contact point $\Delta\boldsymbol{\omega}$ due to the angular velocity $\boldsymbol{\zeta}$ plays a substantial role, meaning that

$$\mathcal{R}_0(a, \lambda, n_0) = -n_0 \int \mathrm{d}\Omega\ (\Delta v_\xi + \Delta\omega_\xi)\ \Theta(-(\Delta v_\xi + \Delta\omega_\xi))\ . \qquad (4.14)$$

The indicator function is dropped here assuming $\chi \approx 1$. An example of the situation is shown in figure 4.7.
So even if a particle enters the previously described surfaces they might still not collide in case they rotate away from each other, i.e. the projection of $\Delta\mathbf{v} + \Delta\boldsymbol{\omega}$ on the normal axis $\hat{\boldsymbol{\xi}}$ is not negative even though the projection of $\Delta\mathbf{v}$ is.
A further difficulty here is that $\hat{\boldsymbol{\xi}}$ at the collision point is no longer parallel to the relative radius $\mathbf{r} = \mathbf{r}_2 - \mathbf{r}_1$. For a canonical ellipse $\mathcal{E}^0$ defined by $\frac{x^2}{\lambda^2 a^2} + \frac{y^2}{a^2} - 1 = 0 \equiv$

$f(x,y)$ it becomes

$$\begin{aligned}\hat{\boldsymbol{\xi}} &= \frac{1}{|\nabla f(x,y)|}\nabla f(x,y) = \frac{1}{\left|\frac{\partial f(x,y)}{\partial x}^2 + \frac{\partial f(x,y)}{\partial y}^2\right|}\begin{pmatrix}\frac{\partial f(x,y)}{\partial x}\\ \frac{\partial f(x,y)}{\partial y}\end{pmatrix}\\ &= \frac{1}{\sqrt{\frac{x^2}{\lambda^4}+y^2}}\begin{pmatrix}\frac{x}{\lambda^2}\\ y\end{pmatrix} = \frac{1}{\sqrt{\frac{\cos^2(u)}{\lambda^2}+\sin^2(u)}}\begin{pmatrix}\frac{\cos(u)}{\lambda}\\ \sin(u)\end{pmatrix},\end{aligned}$$

considering the parametrization of $\mathcal{E}^0$ as in the previous section.
For any vector O its component in this direction is then given by

$$\Delta O_\xi = \hat{\boldsymbol{\xi}}^T \Delta \mathbf{O} = \frac{1}{\sqrt{\frac{\cos^2(u)}{\lambda^2}+\sin^2(u)}}\left(\Delta O_x \frac{\cos(u)}{\lambda} + \Delta O_y \sin(u)\right). \tag{4.15}$$

The translational velocity $\Delta\mathbf{v}$ can usually be solved in the same way as for spherical particles. Especially when advected particles are considered, as this is the case in the thesis, the velocity is approximated by the fluid velocity.

Including rotations one additionally has to solve the velocity $\boldsymbol{\omega}$. The first thing to do is to actually define what is meant by $\boldsymbol{\omega}$. It connects the angular velocity $\boldsymbol{\zeta}$, which indicates how much the angle changes in a given time interval, with a certain point. As rigid bodies are the investigated object, the interesting points are precisely on the surface of the particle and $\boldsymbol{\omega}$ is at every point $\mathbf{r}_s$ on this surface given by the cross product of $\boldsymbol{\zeta}$, which is pointing in the z-direction in the two-dimensional case, and the vector to this point $\mathbf{r}_s$.

$$\boldsymbol{\omega} = \boldsymbol{\zeta} \times \mathbf{r}_s = \begin{pmatrix}0\\0\\\frac{\mathrm{d}\phi}{\mathrm{dt}}\end{pmatrix} \times \begin{pmatrix}x_s\\y_s\\0\end{pmatrix} = \frac{\mathrm{d}\phi}{\mathrm{dt}}\begin{pmatrix}-y_s\\x_s\end{pmatrix} = \frac{\mathrm{d}\phi}{\mathrm{dt}}\begin{pmatrix}-a\sin(u)\\a\lambda\cos(u).\end{pmatrix}$$

Consequently the relative velocity $\Delta\boldsymbol{\omega}$ of two touching ellipses is obtained by

$$\begin{aligned}\Delta\boldsymbol{\omega} = \boldsymbol{\omega}_2 - \boldsymbol{\omega}_1 &= \frac{\mathrm{d}\phi_2}{\mathrm{dt}}\begin{pmatrix}-y_{s2}\\x_{s2}\end{pmatrix} - \frac{\mathrm{d}\phi_1}{\mathrm{dt}}\begin{pmatrix}-y_{s1}\\x_{s1}\end{pmatrix}\\ &= \frac{\mathrm{d}\phi_2}{\mathrm{dt}}\begin{pmatrix}-y_{s1}+y_c\\x_{s1}-x_c\end{pmatrix} - \frac{\mathrm{d}\phi_1}{\mathrm{dt}}\begin{pmatrix}-y_{s1}\\x_{s1}\end{pmatrix}\\ &= \left(\frac{\mathrm{d}\phi}{\mathrm{dt}}\right)\begin{pmatrix}-y_{s1}\\x_{s1}\end{pmatrix} - \frac{\mathrm{d}\phi_2}{\mathrm{dt}}\begin{pmatrix}-y_c\\x_c\end{pmatrix}\end{aligned} \tag{4.16}$$

with the relative angle $\phi = \phi_2 - \phi_1$.
So $\Delta\boldsymbol{\omega}$ does not only depend on the relative orientation and the angular velocity of the two particles when they collide, but also on the individual angles. This all results from the fact that $|\mathbf{r}|$ is not constant any more, like it is for spherical particles where the $\boldsymbol{\omega}_{1/2}$ are always parallel and additionally orthogonal to the $\hat{\boldsymbol{\xi}}$-axis, such that the projection of the superposition $\Delta\omega_\xi$ always vanishes.
In general $\frac{\mathrm{d}\phi}{\mathrm{dt}}$ can be obtained by the Jeffrey equations in spherical coordinates. In easier, however more unrealistic, cases the value will also be a constant only.

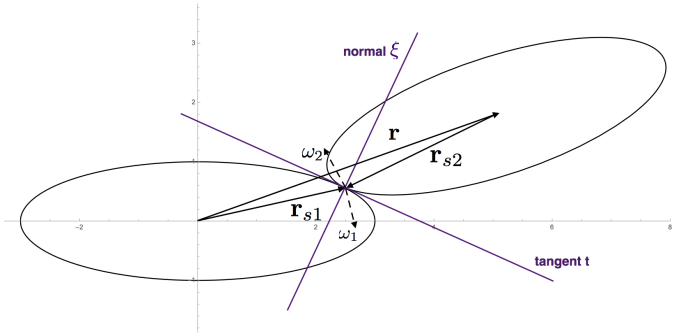

Figure 4.7: Exemplary schematic view of the vectors and directions involved.

Putting all the knowledge gained in the previous abstracts together equation (4.14) can be explicitly written down. For a given relative angle the general collision rate is

$$\begin{aligned}\mathcal{R}_0(n_0, a, \lambda, \phi, \Delta\mathbf{v}, \Delta\boldsymbol{\omega}, \mathbf{r}) = -n_0 \int_0^{2\pi} \mathrm{du}\, P(\phi, \Delta\mathbf{v}, \Delta\boldsymbol{\omega}, \mathbf{r}(u)) \\ \cdot \Delta l\, \frac{(\Delta v_x + \Delta\omega_x)\frac{\cos(u)}{\lambda} + (\Delta v_y + \Delta\omega_y)\sin(u))}{\sqrt{\frac{\cos^2(u)}{\lambda^2} + \sin^2(u)}} \\ \cdot \Theta(-(\Delta v_x + \Delta\omega_x)\frac{\cos(u)}{\lambda} - (\Delta v_y + \Delta\omega_y)\sin(u)).\end{aligned}$$

Note that both Δl (4.10), Δv_i, $\Delta\omega_i$ (depending on the problem) and implicitly $(x_{1s}, y_{1s})^T$ and $\mathbf{r} = (x_c, y_c)^T$ (arbitrary rotation of a canonical ellipse $\mathcal{E}^0$ and respectively (4.8 - 4.9)) are in general dependent on a, λ, u and ϕ. $P(\phi, \Delta\mathbf{v}, \Delta\boldsymbol{\omega}, \mathbf{r}(u))$ is the joint distribution that the particles are at a separation $\mathbf{r}$ such that they touch and that the particles have relative angle ϕ as well as relative translational and rotational velocity $\mathbf{v}$ and $\boldsymbol{\omega}$ at the contact point. Thus, the total one-particle collision rate is

$$\mathcal{R}_0(a, \lambda, n_0) = \iiint \mathrm{d}\phi\, \mathrm{d}\Delta\mathbf{v}\, \mathrm{d}\Delta\boldsymbol{\omega}\, \mathcal{R}_0(n_0, a, \lambda, \phi, \Delta\mathbf{v}, \Delta\boldsymbol{\omega}, \mathbf{r}). \tag{4.17}$$

Depending on the circumstances (4.17) will be adapted. Nonetheless, obviously by including the angular velocity the whole situation becomes more tricky. In many cases it is also not that trivial to get the distribution of relative angles. In the three cases that I investigated I already faced a lot of challenges even though the first two are in particular relatively simple fluid flows.

In summary, in this chapter the used methods and concepts were presented. At first the governing equations that determine the behaviour of spheroids in a fluid flow, the Jeffrey equations, were described. Followed by that it was given an algebraic equation which defines exactly when two spheroids touch. The last part concentrates on the two dimensional problem because there the surfaces that have to be integrated over can be solved analytically by using a geometric condition. Moreover it was seen that the length of those curves does not depend on the relative angle. This result will be used in later calculations.

Last but not least it was described how to include rotations in the actual equation for the collision rate and therefore all needed tools were collected such that in the next chapters I am going to present results for three different fluid flows, the kinetic limit, the shear flow and the random flow.

5

Particles in the kinetic limit

The first system that was investigated consists of N spheroids in a unit box with random velocities $\mathbf{u}^{(i)}$, $i \in 1...N$ sampled from a normal distribution in each dimension. It is therefore nevertheless equally likely to find a particles in a certain direction. In particular two types of systems were studied, non-rotating particles and particles with constant rotation rates $\frac{\mathrm{d}\phi}{\mathrm{dt}}$ and $\frac{\mathrm{d}\theta}{\mathrm{dt}}$.

The assumption that they have a constant velocity is physically related to a very large Stokes number. They keep their movement without noticing an underlying flow. However, in real flows the particles would rather have angular movements, that would moreover be time-dependent, which would definitely have an impact on the collision rate. For now, this is good starting point where the two-dimensional theoretical value can be calculated and compared to the simulations.

5.1 Spherical particles and non-rotating spheroids

The collision rate is the influx through the surface derived in section 4.3. Only negative relative translational velocities contribute now as there are no angular velocities. In the next section this will not be the case any more and they play an important role in the calculations. For now it is sufficient to define the collision rate like in (3.1).

If the velocities are randomly distributed the probability distribution of the relative velocity of two particles $\Delta\mathbf{v} = \mathbf{v}_2 - \mathbf{v}_1$ is needed. In general if two variables are normally distributed with mean μ_1 and μ_2 and variance σ_1 and σ_2 their difference is also normally distributed, however with mean $\mu = \mu_2 - \mu_1$ and variance $\sigma^2 = \sigma_2^2 + \sigma_1^2$. In d dimensions this means

$$P(\Delta\mathbf{v}) = \frac{1}{(\sqrt{2\pi\sigma^2})^d} \exp\left[-\frac{\sum_{j=1}^{d}(\Delta v_j - \mu)^2}{2\sigma^2}\right].$$

The coordinate system is chosen to have one unit vector along the relative position vector $\mathbf{r} = \mathbf{r}_2 - \mathbf{r}_1$ and the rest orthogonal to that. As the direction of the velocities is uniformly distributed, and the choice of the system is only a rotation of the Cartesian coordinates, this can be done without any further problem.

The solutions for the one-particle collision rate with $\mu_2 = \mu_1 = 0$ and $\sigma_2^2 = \sigma_1^2 = \tilde{\sigma}^2$ is calculated below.

$$
\begin{aligned}
R_0(a,\lambda,n_0) =& -n_o \int_\Omega \mathrm{d}\Omega \int \mathrm{d}\Delta\mathbf{v}\ \ P(\Delta\mathbf{v})\ \ \Delta v_r\ \ \Theta(-\Delta v_r) \\
=& -\frac{n_o}{(\sqrt{4\pi\tilde{\sigma}^2})^d} \int_\Omega \mathrm{d}\Omega \int \mathrm{d}\Delta\mathbf{v} \exp\left[-\frac{\sum_{j=1}^d \Delta v_j^2}{4\tilde{\sigma}^2}\right] \Delta v_r \Theta(-\Delta v_r) \\
=& -\frac{n_o}{\sqrt{4\pi\tilde{\sigma}^2}} \int_\Omega \mathrm{d}\Omega \int_{-\infty}^{0} \mathrm{d}\Delta v_r \exp\left[-\frac{\Delta v_r^2}{4\tilde{\sigma}^2}\right] \Delta v_r \\
=& -\frac{n_o}{\sqrt{4\pi\sigma^2}} \int_\Omega \mathrm{d}\Omega\ \ \left(-\frac{1}{2\cdot\frac{1}{4\tilde{\sigma}^2}}\right) = \frac{n_0\tilde{\sigma}}{\sqrt{\pi}} \int_\Omega \mathrm{d}\Omega. \qquad (5.1)
\end{aligned}
$$

The surface integral is the only variable left, as it depends on the shape of the particles. To start with I am going to show the simulation results for spherical particles in comparison to the solution of equation (5.1) before I go over to non-rotating spheroids.

5.1.1 Spherical particles

For spherical particles the integral over the surface Ω is either the circumference of a circle with radius $2a$ with a being the radius of the particles in two dimension or the surface of the sphere with the same radius in three dimensions. Their orientations do absolutely not matter due to their rotational symmetry. The collision rate is easily calculated by

$$
\textbf{2d:} \quad R_0(a,1,n_0) = \frac{n_0}{\sqrt{\pi}} \int \mathrm{d}\Omega = \frac{n_0}{\sqrt{\pi}} \cdot 2(2a)\pi = 4a\sqrt{\pi} n_0 \qquad (5.2)
$$

$$
\textbf{3d:} \quad R_0(a,1,n_0) = \frac{n_0}{\sqrt{\pi}} \int \mathrm{d}\Omega = \frac{n_0}{\sqrt{\pi}} \cdot 4(2a)^2\pi = 16a^2\sqrt{\pi} n_0. \qquad (5.3)
$$

The variance of Δv_r is chosen to be $\tilde{\sigma}^2 = 1$ in all simulations.

Consequently the one-particle collision rate depends linearly on the density and the particle radius in 2d, whereas it depends on a^2 in 3d. The performed simulations confirm these statements (figure 5.1).

This also coincides with what would be expected from basic kinetic gas theory and collision theory [1, 28]. The particle velocities then follow a Maxwell-Boltzmann distribution being proportional to $\exp[-c \cdot v^2]$ like in the upper case. The cross section ($2(2a)$ for $d = 2$ and $(2a)^2\pi$ for $d = 3$) is the determining parameter when it comes to collisions. By the choice of the distribution the prefactor can of course deviate, but the dependencies on the particle radius and the number density are precisely what one gets out the approach used here. Note that in kinetic gas theory the collision process itself is not neglected, but as elastic collisions do not result in a change of the distribution of velocities, both descriptions are equivalent.

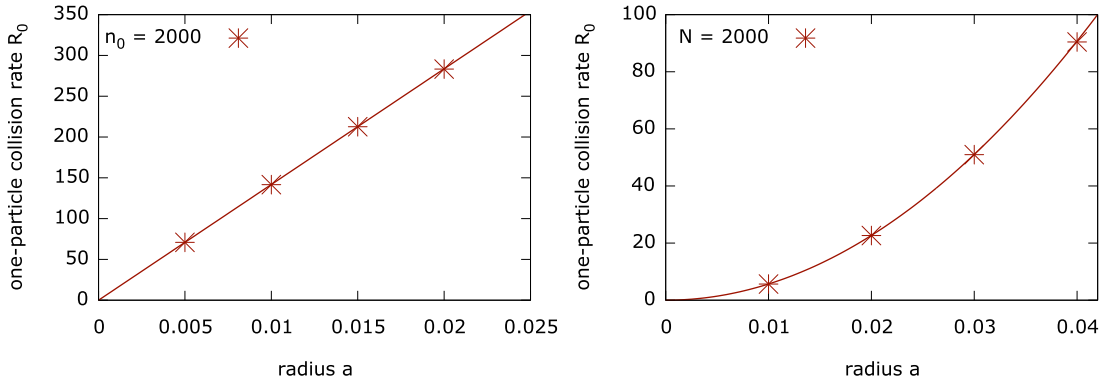

(a) **(b)**

Figure 5.1: One-particle collision rate for spherical particles with radius a with constant random velocity in each direction (Gaussian distributed, $\mu = 0, \sigma = 1$). Uniform initialization. Markers represent the mean of 100 independent simulations. The standard error is too small to be visible. Lines show the theory. (a) 2d simulation with (5.2). (b) 3d simulation with (5.3). Simulation parameters: $n_0 = 2000$, box volume L^d with $L = 1$, $dt = 0.0005$, 5000 time steps.

5.1.2 Spheroids

As shown in section 4.3 the surface that has to be integrated over in the case of axisymmetric particles is a non-trivial function of λ and ϕ. Nevertheless the fact that the length is not dependent on the relative orientation ϕ allows to find analytical expressions here. Only the solutions of $(x_c, y_c)^T$ are available according to (4.8 - 4.9), which is why the theoretical part is limited to two dimensions.

As the orientations are uniform random numbers between 0 and π, and so are the relative orientations due to the periodicity, the one-particle collision rate from (5.1) reduces to

$$\textbf{2d:} \quad R_0(a,\lambda,n_0) = \frac{n_0}{\sqrt{\pi}} \int_0^\pi \mathrm{d}\phi' \int \mathrm{d}\Omega P(\phi') = \frac{n_0}{\sqrt{\pi}} \int \mathrm{d}\Omega \underbrace{\int_0^\pi P(\phi')\mathrm{d}\phi'}_{=1}$$

$$\overset{(4.13)}{=} \frac{n_0}{\sqrt{\pi}} \cdot 4(2a)\lambda E(k^2) = \frac{8}{\sqrt{\pi}} n_0 a \lambda E(k^2) \tag{5.4}$$

with $E(k^2) = E(1 - \frac{1}{\lambda^2})$ being a complete elliptic integral of second kind and a the minor axis of the ellipse. No matter what $P(\phi)$ is, the integral over it will always be one due to the normalization condition. Thus the distribution of the relative orientations is actually irrelevant.
The interesting fact is, and that confirms the latter statement and the assertion made in section 4.3, it does not matter which relative orientations the particles have, the collision rate remains the same. Besides simulations with ellipses with random orientation I checked the cases $\phi_n = 0$ for all ellipses and half of the ellipses

with $\phi_n = 0$ and the other half $\phi_{m\neq n} = \frac{\pi}{2}$. However (5.4) is valid for all possible distributions of relative angles due to the fact that the integrals are the same.

In all simulations ellipses have the same area $A = ac\pi = a^2\lambda\pi = const.$ and therefore the packing density stays constant. Here (5.4) is slightly modified.

$$R_0(A, \lambda, n_0) = \frac{8}{\sqrt{\pi}} n_0 a\lambda E(k^2) = \frac{8}{\sqrt{\pi}} n_0 \sqrt{\frac{A}{\lambda\pi}} \lambda E(k^2) = \frac{8}{\pi} n_0 \sqrt{A\lambda} E(k^2). \tag{5.5}$$

Last but not least the collision rate of ellipses was compared to corresponding rates of circles with a radius equal to the minor and to the major axis. They represent upper and lower bounds to the collision rate of the axisymmetric particles. According to (5.2) those curves are defined by

$$R_0^{\min}(A, \lambda, n_0) = 4\sqrt{\frac{A}{\lambda\pi}} \sqrt{\pi} n_0 = 4\sqrt{\frac{A}{\lambda}} n_0 = R_0 \cdot \frac{\pi}{2\lambda E(k^2)} \tag{5.6}$$

$$R_0^{\max}(A, \lambda, n_0) = 4\lambda\sqrt{\frac{A}{\lambda\pi}} \sqrt{\pi} n_0 = 4\sqrt{A\lambda} n_0 = R_0 \cdot \frac{\pi}{2E(k^2)}. \tag{5.7}$$

with $E(k^2)$ being strictly positive if $a, b > 0$, but ellipses with vanishing or negative semi axes are not physical anyway.

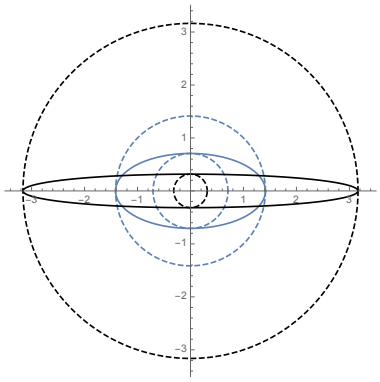

Figure 5.2: Ellipses with their corresponding spherical particles for two different λ (black and blue).

It might be misleading that in figure 5.3 the curves for spherical particles are shown as a function of λ as spherical particles always correspond to $\lambda = 1$. However, in this case the aspect ratio λ is the one that describes the ellipses not the spherical particles. The radii of the spherical particles are precisely chosen such that they depend on this aspect ratio in the previously shown way. Figure 5.3a illustrates the results.
The general proportion of (5.6)-(5.5) to (5.5)-(5.7) for $\lambda > 1$ is

$$\frac{R_0^{\max} - R_0}{R_0 - R_0^{\min}} = \frac{\frac{\pi}{2\lambda E(k^2)} - 1}{1 - \frac{\pi}{2E(k^2)}} < 1.$$

This means that the collision rate for the ellipses in this system has a tendency to be closer to the one for circles with radius λa.
Moreover it is remarkable that the collision rate for growing aspect ratio increases even though the area of the particles stays constant. A possible explanation for that is by making the particles thinner but longer the chance that particles collide increases, because the cross section is in general larger, as can be seen in figure 5.2.

In three dimensions the collision rate does indeed depend on the relative angles of the particles, which can be concluded from the fact that the curves in 5.3b do not coincide. Then the integral over surfaces cannot be exchanged with the integral over ϕ, in contrast to (5.4), and the results differ. All simulated spheroids have the same

volume $V_{(prolate)} = \frac{4}{3}\pi a^3 \lambda_{(prolate)} = const. = V_{(oblate)} = \frac{4}{3}\pi \frac{a^3}{\lambda^2_{(oblate)}}$. Together with (5.3) the curves for spherical particles that were compared with are:

$$R_0^{(1)}(V,\lambda,n_0) = 16\left(\frac{3V}{4\pi\lambda}\right)^{\frac{2}{3}}\sqrt{\pi}n_0 \;\hat{=}\; \begin{cases}\text{prolate: min}\\ \text{oblate: max}\end{cases} \tag{5.8}$$

$$R_0^{(2)}(V,\lambda,n_0) = 16\left(\frac{3V\lambda^2}{4\pi}\right)^{\frac{2}{3}}\sqrt{\pi}n_0 \;\hat{=}\; \begin{cases}\text{prolate: max}\\ \text{oblate: min}\end{cases} . \tag{5.9}$$

The simulations show that also here the collision rate grows by increasing (prolate spheroids) or decreasing (oblate spheroids) the aspect ratio and additionally tends to be closer to spherical particles with $r = a$. Additionally the initial condition has a smaller effect on the collision rate of oblate spheroids than of prolate ones.

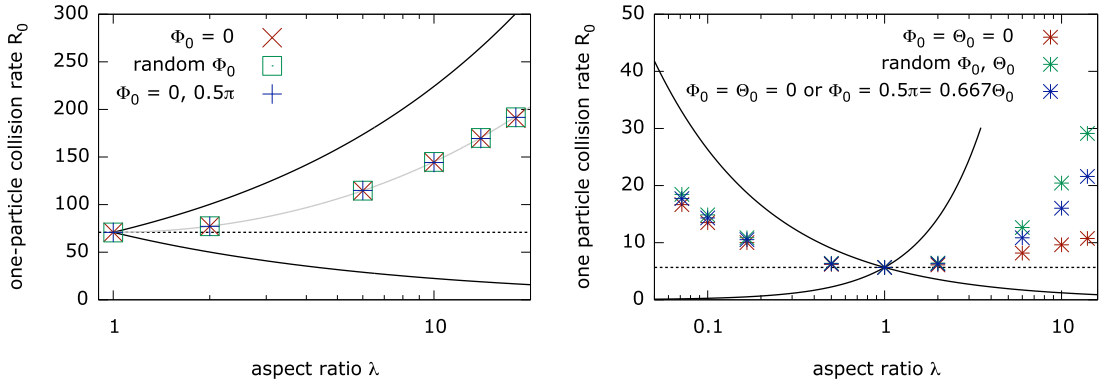

(a) **(b)**

Figure 5.3: One-particle collision rate for non-rotating elliptical particles with aspect ratio λ and constant random velocity in each direction (Gaussian distributed, $\mu = 0, \sigma = 1$) for different initial conditions. Markers represent the mean of 100 independent simulations. The standard error is too small to be visible. Lines show the theory. The black lines illustrate the curves for the corresponding spherical particles with radius $a = \sqrt{\frac{A}{\lambda\pi}}$ and λa (2d) or $a = \left(\frac{3V}{4\lambda\pi}\right)^{\frac{1}{3}}$ and λa (3d) according to (5.6 - 5.9). Dashed lines emphasize the value for $\lambda = 1$. (a) 2d simulation together with (5.5), particle area $A = 0.005^2\pi$. (b) 3d simulation, particle volume $V = \frac{4}{3}\cdot 0.01^3\pi$. Simulation parameters: $n_0 = 2000$, box volume L^d with $L = 1$, $dt = 0.0005$, 5000 time steps.

5.2 Spheroids with a constant rotation rate

Letting the particles rotate adds another degree of freedom to the system. For now it is assumed that the rotation rate $\dot{\phi}_n$ is constant in time for each particle n.
$\mathcal{R}_0$ is given by equation (4.17). However, some more simplifications can be done by choosing the distributions of Δv_i and $\Delta\omega_i$. In particular there are two cases that were investigated.

In the first case, to simplify the situation, the translational velocity is set to 0. Therefore only the rotational movement contributes to the collision rate. The rotation rate is chosen constant and either the same for all particles or it is sampled from a normal distribution with mean $\mu = 0$ and variance $\sigma^2 = \pi$. The system itself is not physically relevant but still it gives rise to a better understanding of the equations as well as helps to test the simulation code, because the theoretical equations do exist. As the angles are initially distributed randomly and furthermore stay distributed randomly $P(\phi) = \frac{1}{\pi}$. $\Delta\omega_\xi$ is a complicated function given by (4.16) depending on u, $\dot{\phi}_1$, $\dot{\phi}_2$ and ϕ.

$$\begin{aligned}\mathcal{R}_0(a,\lambda,n_0) &= -n_0 \int \mathrm{d}\phi \int \mathrm{d}\Omega \int \mathrm{d}\dot{\phi}_1 \int \mathrm{d}\dot{\phi}_2 \; P(\phi,\dot{\phi}_1,\dot{\phi}_2) \; \Delta\omega_\xi \; \Theta(-\Delta\omega_\xi) \\ &= -\frac{n_0}{\pi} \int_0^\pi \mathrm{d}\phi \int_0^{2\pi} \mathrm{du} \int_{-\infty}^{\infty} \mathrm{d}\dot{\phi}_1 \int_{-\infty}^{\infty} \mathrm{d}\dot{\phi}_2 \; \Delta\omega_\xi \; \Theta(-\Delta\omega_\xi) \\ &\quad \cdot \begin{cases} \delta(\dot{\phi}_1 - c_1)\cdot\delta((\dot{\phi}_2 - \dot{\phi}_1) - c_2) & \text{if } \dot{\phi}_1 = c_1, \dot{\phi}_2 - \dot{\phi}_1 = c_2 \\ \frac{1}{2\pi^3}\exp\left[-\frac{\dot{\phi}_1^2+\dot{\phi}_2^2}{2\pi^2}\right] & \text{if sampled rotation rates} \end{cases}\end{aligned} \tag{5.10}$$

In the second case the particles will also have a constant velocity sampled from a normal distribution with $\mu = 0, \sigma^2 = 1$. Then

$$\begin{aligned}&\int \mathrm{d}\Delta v_\xi \; P(\Delta v_\xi) \; (\Delta v_\xi + \Delta\omega_\xi) \; \Theta(-(\Delta v_\xi + \Delta\omega_\xi)) \\ &\quad = \int_{-\infty}^{\Delta\omega_\xi} \mathrm{d}\Delta v_\xi \; \frac{1}{\sqrt{4\pi}} \exp\left[-\frac{\Delta v_\xi^2}{4}\right] \; (\Delta v_\xi + \Delta\omega_\xi) \\ &\quad = \int_{-\infty}^{\Delta\omega_\xi} \mathrm{d}\Delta v_\xi \; \frac{1}{\sqrt{4\pi}} \exp\left[-\frac{\Delta v_\xi^2}{4}\right] \; \Delta v_\xi + \Delta\omega_\xi \int_{-\infty}^{\Delta\omega_\xi} \mathrm{d}\Delta v_\xi \; \frac{1}{\sqrt{4\pi}} \exp\left[-\frac{\Delta v_\xi^2}{4}\right] \\ &\quad = -\frac{1}{\sqrt{\pi}} \exp\left[-\frac{\Delta\omega_\xi^2}{4}\right] + \frac{\Delta\omega_\xi}{2} \operatorname{erfc}\left[\frac{\Delta\omega_\xi}{2}\right],\end{aligned}$$

and therefore analogous to (5.10)

$$\begin{aligned}\mathcal{R}_0(a,\lambda,n_0) &= \frac{n_0}{\pi} \int_0^\pi \mathrm{d}\phi \int_0^{2\pi} \mathrm{du} \int_{-\infty}^{\infty} \mathrm{d}\dot{\phi}_1 \int_{-\infty}^{\infty} \mathrm{d}\dot{\phi}_2 \; \left[\frac{1}{\sqrt{\pi}} \exp\left[-\frac{\Delta\omega_\xi^2}{4}\right] - \frac{\Delta\omega_\xi}{2} \operatorname{erfc}\left[\frac{\Delta\omega_\xi}{2}\right]\right] \\ &\quad \cdot \begin{cases} \delta(\dot{\phi}_1 - c_1)\cdot\delta((\dot{\phi}_2 - \dot{\phi}_1) - c_2) & \text{if } \dot{\phi}_1 = c_1, \dot{\phi}_2 - \dot{\phi}_1 = c_2 \\ \frac{1}{2\pi^3}\exp\left[-\frac{\dot{\phi}_1^2+\dot{\phi}_2^2}{2\pi^2}\right] & \text{if sampled rotation rates} \end{cases}.\end{aligned} \tag{5.11}$$

All results are presented in figures 5.4 - 5.5.

First of all, for rotating particles with no translational velocity the collision rate increases by increasing λ, because of the rotation the effective cross section grows

and thus the chance that particles collide. Depending on the actual $\dot{\phi}$ the change of the collision rate with respect to λ is bigger or smaller. Spherical particles will naturally never collide. In general it is sufficient to simulate one period of the movement because then the movement just repeats and the statistics stay the same.

Therefore the 2d theory coincides very well with the simulation if the rate is a constant for all particles and one can define the period easily, but it deviates considerably if the rate is sampled. Here another problem was faced in the simulations. When $\dot{\phi}$ follows a normal random distribution the effect of quasi periodicity affects the result a lot as the simulation time is limited and it is hard to find a time where all particles have passed one period as the relative period of two particles $\phi_2 - \phi_1$ could be large or even infinite. Some particles will have passed several periods while others have not even completed one. So the stationary collision rate can actually only be covered in infinite time and this could explain why the measured collision rate is deviating. The effect is smaller if λ is close to 1.

In three dimensions the particles not only have a constant $\dot{\phi}$ but also $\dot{\theta}$, which are similarly chosen as in two dimensions. The effect of quasi periodicity is also expectable here, which is why it can be assumed that the simulation results presented in figure 5.4b are again deviating from reality in the case of random sampling of $\dot{\phi}$ and $\dot{\theta}$, whereas this should not be the case $\dot{\phi} = \dot{\theta} = \pi$.

Including a translational velocity $\mathbf{v}$ in the test case the effect can be neglected because it is not leading anymore. Here it was observed that the collision rate does not change by distributing the rotation rates differently. This holds even in 3d where the surfaces are not equally big, as discussed in the previous section.

One can conclude that the integrations from (5.11) are redundant and the whole equation collapses to (5.5). Only numerical errors have led to some deviation.

Figure 5.5 presents this result. By dividing the collision rate by n_0 this plot also supports the linear dependency on n_0 as even those data points collapse to the same value.

This can be explained by the symmetry of the whole system. The velocities are sampled randomly without favouring any direction, and as all particles have the same preconditions the stationary collision rate should on average be the same, particularly not affected by the velocity, the rotation rate or the initialization, as seen before. Nevertheless it is a remarkable result because it would have been intuitive that if particle rotate extremely fast they effectively act like spherical particles with radius λa (ellipses, prolate spheroids) respectively $\frac{a}{\lambda}$ (oblate spheroids) and moreover that it does not make a difference if particles do not rotate at all or with a certain rate. But as the simulations and calculations show, it is not the case. Furthermore it is striking that in all situations oblate spheroids collide less often compared to prolate ones with the same axis lengths. Keeping the volume constant disks with $\lambda_{oblate} = \frac{a}{c}$, $a < c$, will always have a bigger surface than rods with $\lambda_{prolate} = \frac{1}{\lambda_{oblate}} = \frac{c}{a}$ and the ratio grows with increasing $|\Lambda|$. This would rather point towards a higher collision rate.

Concluding, in all cases by increasing the shape factor $|\Lambda|$ the collision rate grows. This holds both for non-rotating and rotating particles in the kinetic limit.

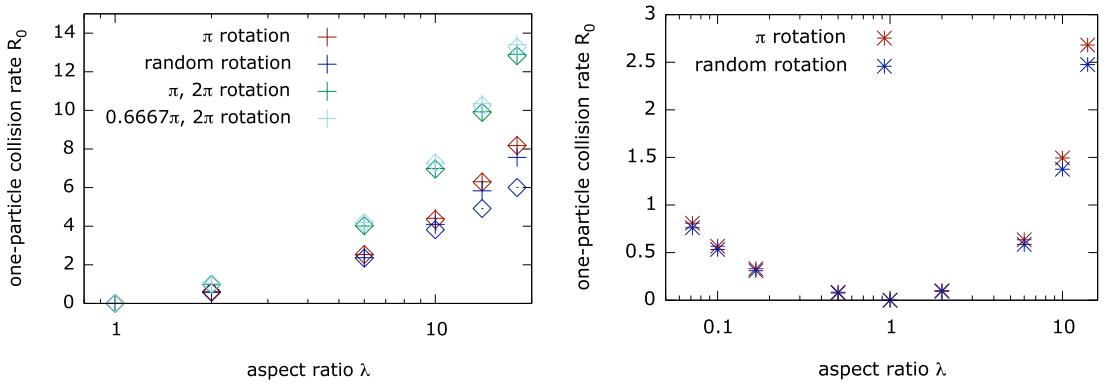

(a) **(b)**

Figure 5.4: One-particle collision rate for elliptical particles with aspect ratio λ with no translational velocity and different choices of constant rotation rates. Random rotation rate refers to a normal random number with mean 0 and standard deviation π for $\dot{\phi}$ and $\frac{\pi}{2}$ for $\dot{\theta}$. Crosses represent the mean of 100 independent simulations. The standard error is too small to be visible. Diamonds show the respective theory. (a) 2d simulation with (5.10) for different c_1, c_2, particle area $A = 0.005^2\pi$. (b) 3d simulation, particle volume $V = \frac{4}{3}0.01^3\pi$. Simulation parameters: $n_0 = 2000$, box volume L^d with $L = 1$, $dt = 0.0005$, $\frac{T}{dt}$ or 5000 time steps.

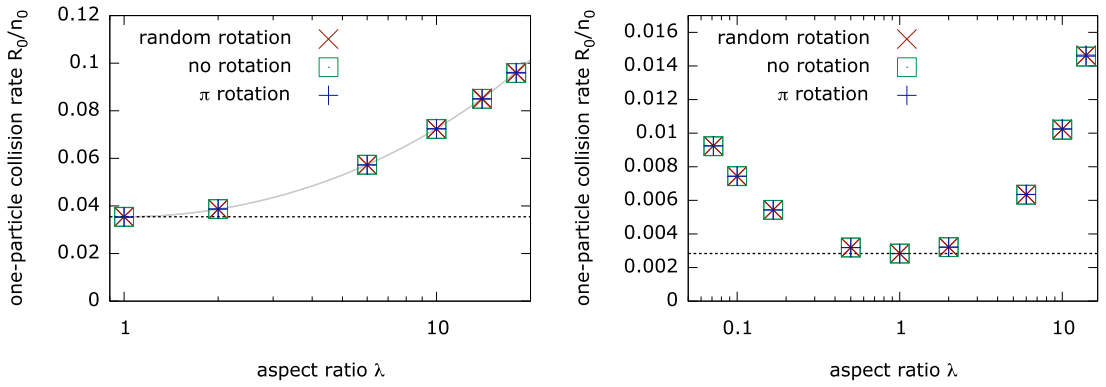

(a) **(b)**

Figure 5.5: One-particle collision rate for elliptical particles with aspect ratio λ with constant random velocity in each direction (Gaussian distributed, $\mu = 0$, $\sigma = 1$) and different choices of constant rotation rates or particle numbers. Random rotation rate refers to a normal random number with $\mu = 0$ and $\sigma = \pi$. Markers represent the mean of 100 independent simulations. The standard error is too small to be visible. Lines show the theory. Dashed lines emphasize the value for $\lambda = 1$. (a) 2d simulation with (5.11), particle area $A = 0.005^2\pi$. (b) 3d simulation, particle volume $V = \frac{4}{3}0.01^3\pi$. Simulation parameters: box volume L^d with $L = 1$, $dt = 0.0005$, $\frac{T}{dt}$ or 5000 time steps.

6

Advected spheroids in the shear flow

Collisions between spherical particles with vanishing St in a shear flow with shear rate s were already discussed in section 3.2.1. In this chapter spheroids under the same conditions are investigated. The translational movement is still fairly easy and moreover uniform. However, the particles start tumbling, i.e. the vector $\mathbf{n}(t)$ along the symmetry axis changes. As introduced in section 4.1 the tumbling is determined by Jeffery's equations, which simplify to

$$\begin{aligned}
\frac{\mathrm{d}\mathbf{r}}{\mathrm{dt}} &= \mathbf{u}(\mathbf{r},t) = \begin{pmatrix} sy \\ 0 \\ 0 \end{pmatrix} \\
\frac{\mathrm{d}\mathbf{n}}{\mathrm{dt}} &= \mathbb{O}\mathbf{n}(t) + \Lambda\left(\mathbb{S}\mathbf{n}(t) - \mathbf{n}(t)\mathbf{n}^T(t)\mathbb{S}\mathbf{n}(t)\right) \\
&= \begin{pmatrix} 0 & \frac{s}{2} & 0 \\ -\frac{s}{2} & 0 & 0 \\ 0 & 0 & 0 \end{pmatrix}\mathbf{n}(t) + \Lambda\left[\begin{pmatrix} 0 & \frac{s}{2} & 0 \\ \frac{s}{2} & 0 & 0 \\ 0 & 0 & 0 \end{pmatrix}\mathbf{n}(t) - \mathbf{n}(t)\mathbf{n}^T(t)\begin{pmatrix} 0 & \frac{s}{2} & 0 \\ \frac{s}{2} & 0 & 0 \\ 0 & 0 & 0 \end{pmatrix}\mathbf{n}(t)\right] \\
&= \frac{s}{2}\begin{pmatrix} n_y\left(1+\Lambda(1-2n_x^2)\right) \\ n_x\left(-1+\Lambda(1-2n_y^2)\right) \\ -2\Lambda n_x n_y n_z \end{pmatrix}
\end{aligned}$$

in the shear flow. The shear is chosen to be in the y-direction as it was in section 3.2.1, but in general choosing any direction is equivalently. In two dimensions the motion in the z-direction is neglected. The shape factor Λ is the parameter that is used in the Jeffery equations instead of the aspect ratio λ. As $\Lambda = \frac{\lambda^2-1}{\lambda^2+1}$, both descriptions are equivalent.
Using the spherical coordinates ϕ and θ $\dot{\mathbf{n}}$ can be rewritten according to (4.2 - 4.3).

$$\dot{\phi} = \frac{s}{2}\left(-1+\Lambda\cos(2\phi)\right) \tag{6.1}$$

$$\dot{\theta} = s\Lambda\sin(\theta)\cos(\theta)\sin(\phi)\cos(\phi) = \frac{s}{4}\Lambda\sin(2\theta)\sin(2\phi). \tag{6.2}$$

(6.1 - 6.2) represent what was described earlier in section 4.1 that particles tumble on stable periodic orbits with period time

$$T = \frac{4\pi}{s\sqrt{1-\Lambda^2}}. \tag{6.3}$$

In the following I explain how particles in a shear flow act in more detail as this is a crucial part in understanding the behaviour of the collision rate with respect to the aspect ratio.

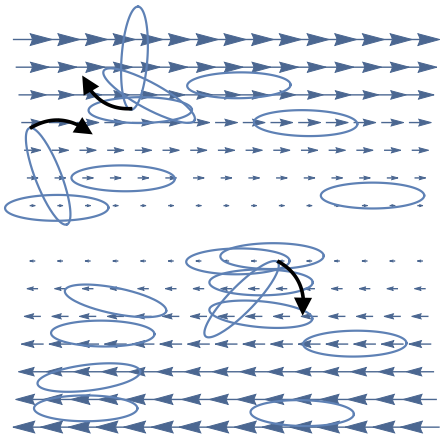

(a) Two-dimensional Jeffrey orbits in shear flow.

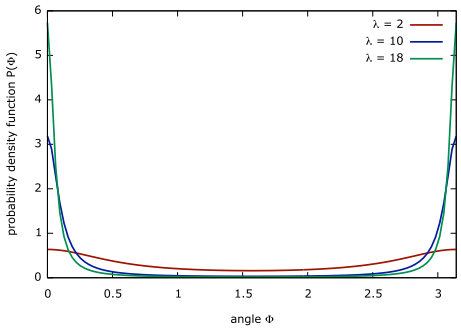

(b) PDF of angles Φ.

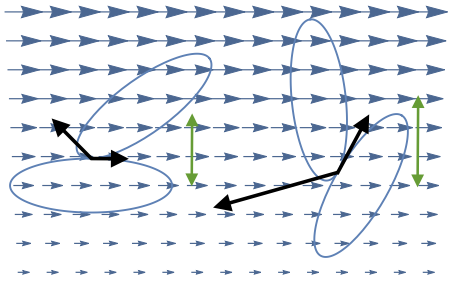

(c) Exemplary scheme of the differences in Δy (green) and $\boldsymbol{\omega}_i$ (black) depending on the orientation in the flow while having the same relative angle and touching point.

Figure 6.1

One can observe that the shape factor Λ has an important impact on the period length T. The bigger its absolute value is the longer the period will be. In the limiting cases where $|\Lambda| = 1$, there is even a stable steady state, i.e. it exists a value for ϕ and θ such that $\dot{\phi} = \dot{\theta} = 0$ and moreover $T \to \infty$.
In particular, this is the case for $\phi^* = k\pi$, $k \in \mathbb{Z}$, for ellipses and rods, and $\phi^* = \left(\frac{1}{2} + k\right)\pi$ for disks. In those cases $\dot{\theta} = 0$ follows automatically, no matter what θ actually is.
Furthermore $\theta^* = k\frac{\pi}{2}$ will also lead to $\dot{\theta} = 0$ for any Λ and ϕ (however $\dot{\phi}$ is not necessarily 0). This is very special case actually corresponding to the two-dimensional situation when cutting through the x-y-plane, in which all particles then lie.

In other words ellipses will prefer to have $\mathbf{n}$ parallel to the velocity field, referred to being aligned. Sooner or later (depending on Λ) they will flip around. This is shown in figure 6.1a. Infinitely long particles will stay in this state as soon as they reach it. For each aspect ration there is only one Jeffery orbit that the particles follow.

Rods and disks move on different Jeffrey orbits illustrated in 4.1 determined by the initial condition. Infinitely long and thin rods will end up in a steady state where ϕ is a multiple of π but θ can in general be everything. The same holds for disks except that ϕ is a multiple of π added to $\frac{\pi}{2}$. Keep in mind that the $\mathbf{n}$ vector is along the symmetry axis of the particle, which results in this shift. Disks therefore have their thin side facing the flow, rods their 'nose'. Nevertheless finite particles always have a periodic movement in the third dimension, which potentially gives rise to much more collisions.

In the following I only proceed the calculations in 2d. However, the simulated 3d

results are presented afterwards, which is why it is essential to understand the behaviour and limits there as well.
By solving the Fokker-Planck equation [25] the stationary probability density function of ϕ of this dynamical system can be obtained. As everything is deterministic the diffusion part can be neglected and it simplifies to

$$0 \stackrel{!}{=} \frac{\partial P(\phi)}{\partial t} = -\frac{\partial}{\partial \phi}(\dot{\phi} P(\phi)) + \cancel{\mathcal{D}\frac{\partial^2 P(\phi)}{\partial \phi^2}} = -P(\phi)\frac{\partial \dot{\phi}}{\partial \phi} - \dot{\phi}\frac{\partial P(\phi)}{\partial \phi}. \tag{6.4}$$

(6.4) can easily be solved and with the probability normalized to unity the distribution is given by

$$P(\phi) = \frac{1}{\pi} \cdot \frac{\sqrt{1-\Lambda^2}}{1 - \Lambda\cos(2\phi)}. \tag{6.5}$$

(6.5) not only proofs that ellipses in the shear flow tend to be aligned with the flow, but also it is an important factor in the calculation of the theoretical collision rates. Now both the translational and rotational velocities can be determined by the equations presented above. There is no random component anymore. However, now it does not only play an important role which relative orientation the particles have but also which individual orientations they have. For instance, for a given relative angle two particles can have both different relative positions Δy, which influences $\Delta \mathbf{v}$, and also different $\dot{\mathbf{n}}$ depending on how the particles lie relative to the flow direction (see figure 6.1).
Thus the collision rate should depend on the initial condition, because the movement after the initialization is only dependent on the shape (which is the same for all particles). For some chosen initializations

$$\begin{aligned}
\mathcal{R}_0(a,\lambda,n_0) &= -n_0 \int \mathrm{d}\phi_1 \int \mathrm{d}\phi_2 \int \mathrm{d}\Omega \;\; P(\phi_1,\phi_2) \\
&\quad \cdot (\Delta v_\xi + \Delta\omega_\xi) \;\; \Theta(-(\Delta v_\xi + \Delta\omega_\xi)) \\
&= -n_0 \int \mathrm{d}\phi_1 \int \mathrm{d}\phi_2 \int \mathrm{d}\Omega \;\; (\Delta v_\xi + \Delta\omega_\xi) \;\; \Theta(-(\Delta v_\xi + \Delta\omega_\xi)) \\
&\quad \cdot \begin{cases} \delta(\phi_2 - \phi_1) \cdot P(\phi_1) & \text{if } \phi_0 = 0 \\ P(\phi_1) \cdot P(\phi_2) & \text{if } \phi_0 \text{ random} \end{cases} .
\end{aligned} \tag{6.6}$$

It was obtained a decreasing collision rate with increasing aspect ratio, keeping the area constant. On the one hand particles will more and more be aligned and the flipping will happen much faster. On the other hand particles that are thinner but longer also have the chance to hit a lot more particles while turning. In the end it is a balance between those two mechanisms. However, for $\lambda \to \infty$ the collision rate should approach the one for spherical particles with a radius that is equivalent to the minor axis a of the ellipse, and should naturally vanish while $a \to 0$.

All in all I investigated two different cases, either particles have a random initial angle or all start at $\phi_0 = 0$. The latter automatically induces that particles will have the same angle at any time (according to (6.1 - 6.2)) and consequently the relative angle between the particles vanishes at all times simplifying (6.6) further (implicitly

Δv_ξ and $\Delta\omega_\xi$). Despite that it is again an unphysical assumptions, it is easier to calculate and helps to understand the system. In the limit $\lambda \to \infty$ the two cases should however coincide. Figure 6.2 present the main results.
In the simulations the behaviour explained above can be observed very well in 2d. The collision rates approach the curve for spherical particles with radius $a = \frac{A}{\lambda\pi}$ and eventually zero. The numerical solution of (6.6) can be reproduced by the simulations. In the case where all particles are initially randomly distributed it is not the case for unclear reasons. The simulated collision rate is systematically smaller than the solution of the integral.
It does indeed make sense that the simulation tends to underestimate the actual collision rate for growing aspect ratios as the time steps are kept constant and the periods will increase. In general it is reasonable to let the simulation run for a certain time that is defined by a multiple of T (in my simulations I used exactly one period). Only then the full statistics can be covered. Especially for high aspect ratios, where the particles are aligned with high probability, it makes a big difference if one stops the simulation earlier. Simulations up till $\lambda = 18$ were performed, but until then the deviations can definitely not be explained by that.
However, with the latter choice of initialization the solution of the numerical integration of (6.6) seems to be unstable, which becomes apparent especially for large aspect ratios, where the theoretical curve shows fluctuations. Therefore one might also suspect that the numerical solution of the integral using Mathematica is responsible for the deviation, but in order to give a profound reason further investigations are required. However, there is no other explanation so far.

In three dimensions the collision rate does not approach zero with increasing aspect ratio, because the Jeffery orbits in 3d allow a lot more collisions, especially for long or big particles, and moreover the particles will move on orbits according to their initial condition, whereas in 2d they all follow the same orbit only with a possible time shift. I investigated the collision rate for some defined initial conditions as well as a random initialization. It can be seen that besides the shape the initial condition has a big influence to the collision rate, which is expected. A very special case though is $\phi_0 = \theta_0 = 0$ where the collision rate is just a constant, not depending on the aspect ratio. However, this is a very trivial case as then $\dot{\theta}$ vanishes. There is still a motion in ϕ direction but as $\theta = 0$ it corresponds to a rotation around the symmetry axis, and consequently it is not noticeable. There is only the one-dimensional translational movement that counts. Because the volume of the particles is constant, changing the aspect ratio makes them thicker in one direction but thinner in the other, which is why in total the collision rate stays constant. Furthermore there is no general connection between rods and disks with the same axis lengths a and λa.

Finally, the simulations confirm the theory in two dimensions, predicting that the collision rate will approach 0 with increasing aspect ratio, however there is a systematic deviation when the particles are initialized randomly that is probably a consequence of the unstable numerical solution. Moreover the initial condition influences the rate even though given a λ all particles follow the same Jeffery orbit. In three dimensions the collision rate in contrast increases for increasing shape factor $|\Lambda|$. The initial condition has an even higher impact on $\mathcal{R}_0$ as it also determines according to which Jeffery orbit the particle rotates.

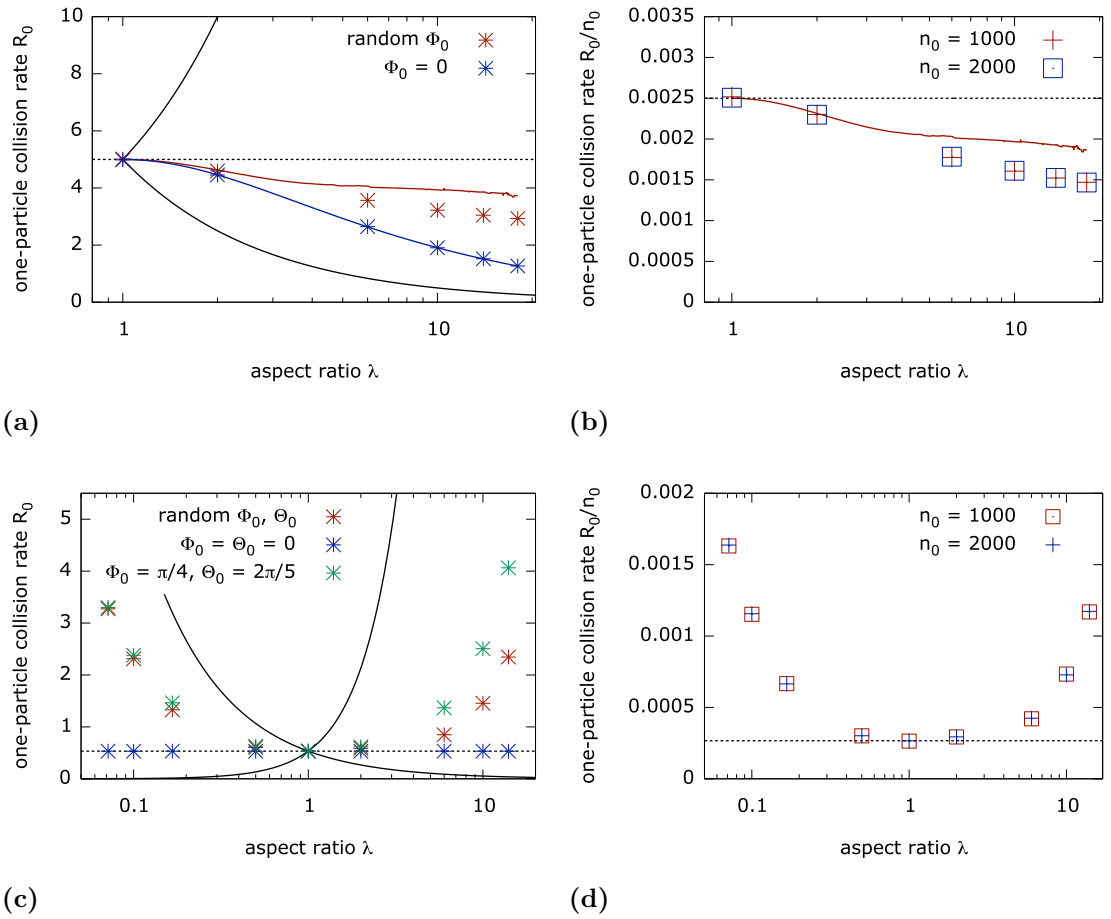

Figure 6.2: One-particle collision rate for elliptical particles with aspect ratio λ in the shear flow. Markers represent the mean of 100 independent experiments. The standard error is too small to be visible. Lines show the theory. The black lines illustrate the curves for the corresponding spherical particles with radius $a = \sqrt{\frac{A}{\lambda\pi}}$ and λa (2d) or $a = \left(\frac{3V}{4\lambda\pi}\right)^{\frac{1}{3}}$ and λa (3d) according to (3.4 - 3.5). The dashed lines emphasize the value for $\lambda = 1$. (a) 2d simulation for different initializations with (6.6), particle area $A = 0.005^2\pi$, $n_0 = 2000$. (b) 2d simulation divided by n_0 for different particle number densities with (6.6), particle area $A = 0.005^2\pi$, uniform initialization. (c) 3d simulation for different initializations, particle volume $V = \frac{4}{3}0.01^3\pi$, $n_0 = 2000$. (d) 3d simulation divided by n_0 for different particle number densities, particle volume $V = \frac{4}{3}0.01^3\pi$, uniform initialization. Simulation parameters: $s = 25$, box volume L^d with $L = 1$, $dt = 0.0005$, $\frac{T(\lambda)}{dt}$ time steps.

7

Advected spheroids in the random flow

The last case that I am going to describe is a flow that is a statistical model for small scales in turbulence which was already presented in chapter 3.
On the one hand it is the most interesting case in this thesis, but at the same time it is also the most difficult case. The equation of motion is fully determined by the assumption that the particles are advected ($\mathbf{v}(\mathbf{r},t) = \mathbf{u}(\mathbf{r},t)$) together with the corresponding Jeffery equations from (4.2 - 4.3). The random flow is constructed precisely as described in appendix A. In each time step the flow has to be evaluated for every particle at a certain position $\mathbf{r}$. This is a very time consuming procedure. As shown in the appendix A the flow velocities and gradients are the result of a random Gaussian function that takes into account a certain number of Fourier modes depending on the box length L, the correlation length η and the desired precision p (equation (A.4)).

It is important to find a balance between the right choice of parameters according to the time and length scales in the system and computation time. In the derivation of the flow it was assumed that $L \gg \eta$. Additionally $a, c \ll \eta$. For instance, in a unit box and $\eta = 0.1$ there are 10 Fourier modes that have to calculated for each dimension (precision of 8 digits). Influencing the number of Fourier modes corresponds to increasing η or decreasing L. As the focus lies on the collision rate, it is more reasonable to chose the second alternative, because then particles collide more often and the statistics become better. At the same time it is important to not decrease it too much as then the flow will not be fully isotropic anymore and additionally the correlation functions will no longer agree with what would be expected, because the length scales of the system are too similar.
Both in figure A.1 ($\langle A_{xx}(0,0)A_{xx}(\mathbf{r},0)\rangle$) and in 7.1 ($\mathcal{R}_0$) it was confirmed that $L = 0.5$ is a good compromise, even though one has to keep in mind that especially for big distances compared to the particle size the correlations are not represented sufficiently good by this choice, but as collisions happen at small distances the collision rate is not significantly influenced. The number of Fourier modes that has to be calculated for each dimension drops to 5, which results in a significant gain in computation time.

It is not straight forward to include all the facts and properties of the random flow in the equation for the collision rate, because it cannot be reasoned in the same way as in section 3.2.2 as the problem is not symmetric in all directions any longer. Because the flow is ideally homogeneous and isotropic it is nevertheless expected that the

stationary spatial distribution is uniform, and the same holds for the distribution of angles. Eventually there is no theory to compare with and only simulation results are presented which still give an idea of how the collision rate changes with respect to the shape.

In two spatial dimensions by increasing the aspect ratio and keeping the particle area constant the collision rate first drops and then increases again according to figure 7.1. This can be the result of different behaviours that are more or less distinctive for different shapes.
The drop of the collision rate indicates that there could be some sort of alignment, like it happened in the shear flow, leading to a decrease of the collision rate as the minor axis becomes smaller. But at the same time the larger the aspect ratio becomes the more the effect of the fluctuations of the flow could encourage collisions due to the fact that particles recollide in a short period of time, which is related to the function χ described when the collision rate was introduced, and which is actually an unwanted behaviour that should not be included in the collision rate. Also thinking about an axisymmetric particle moving along a vortex it seems reasonable that a very elongated particle would get the chance to hit more particles than an approximately spherical one, especially when it rotates at the same time. By further increasing λ the latter two effects might be more significant than the alignment and therefore the collision rate increases again.
Furthermore the simulations confirm a linear dependency on the particle number density n_0, however the dependency on the Kubo number Ku and the particle area A are not linear anymore. In chapter 3 it was seen that for spherical particles the collision rate is direct proportional on Ku and A, which is also validated by all simulations for $\lambda = 1$. When the aspect ratio is close to 1 linear dependencies appear to be a good approximation though.

Simulated collision rates in three dimensions are presented in figure 7.2. The biggest problem faced here is the computation time. All in all it was only possible to produce results for one independent experiment. Therefore it is questionable if the results resemble the actual collision rates, but in previous cases it was observed that 100 independent experiments are actually more than necessary and the standard error is extremely small, which supports at least the tendencies that are illustrated in figure 7.2.
The main observation that can be made is that the collision rate increases by increasing $|\Lambda|$ while oblate spheroids collide less often than prolate ones. With only one simulation it is not possible to make a proper statement on the dependencies on Ku, n_0 or V, but at least the simulation points to support the hypothesis made for the two-dimensional system.

In general it is qualitatively not completely understood how axisymmetric particles move in the random flow, as there are no deterministic equations like there are in the shear flow, for example. To study the collision rate can give hints to what happens but in many cases it is a superposition of different effects so that in the end it is hard to find a definite explanation, but only speculations. One can nevertheless conclude that the shape, i.e. Λ, has a great impact on the collision rate and leads in general to an increase the more elongated the particle are if the volume is kept constant.

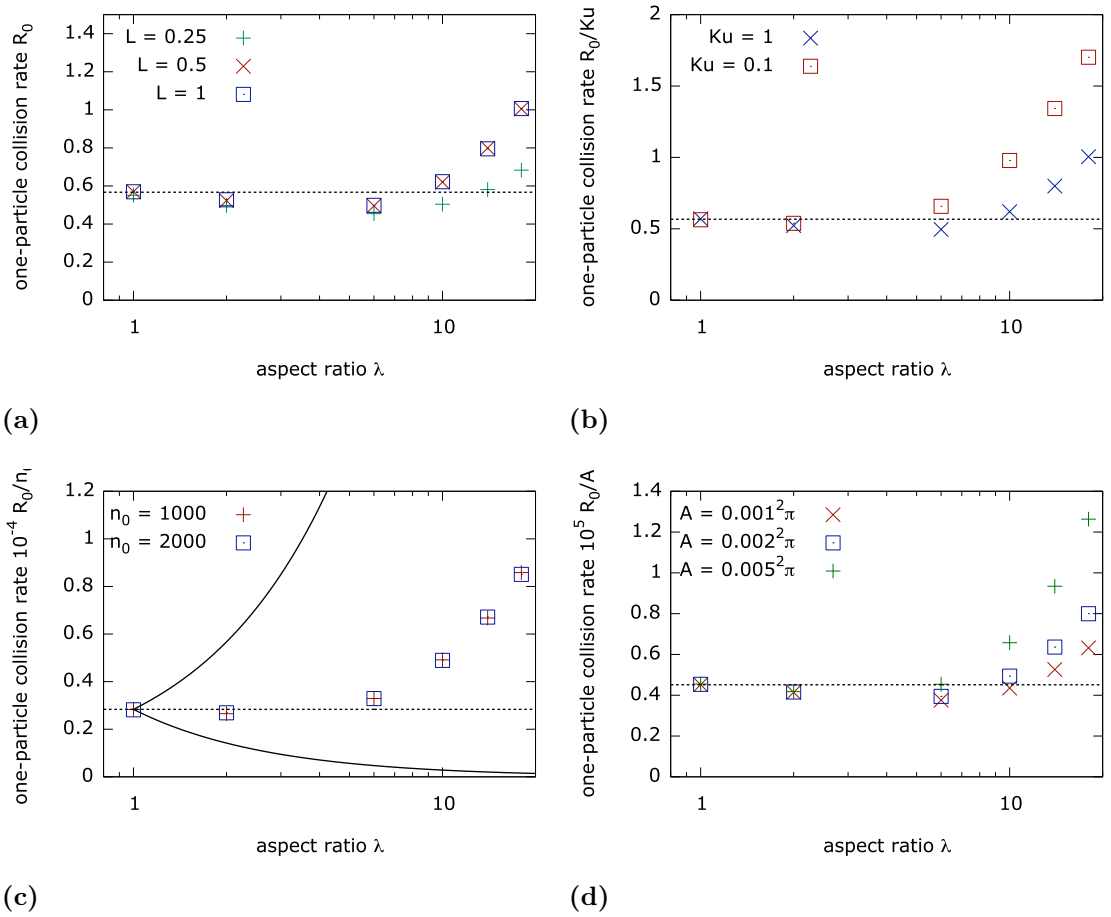

Figure 7.1: One particle collision rate for two-dimensional elliptical particles with aspect ratio λ in the random flow. Random initialization of positions and angles. Markers represent the mean of 100 independent experiments. The standard error is too small to be visible. The black lines illustrate the curves for the corresponding spherical particles with radius $a = \sqrt{\frac{A}{\lambda\pi}}$ and λa according to (3.8). The dashed lines emphasize the value for $\lambda = 1$. (a) Effect of the box length L, Ku= 1, $A = 0.002^2\pi$, $n_0 = 2000$. (b) Effect of the Kubo number Ku, $L = 0.5$, $A = 0.002^2\pi$, $n_0 = 2000$. (c) Effect of the particle number density, $L = 0.5$, $A = 0.002^2\pi$, Ku= 0.1. (d) Effect of the particle area A, $L = 0.5$, Ku= 0.1, $n_0 = 2000$. Further simulation parameters: $\eta = 0.1$, $\tau = 0.1$, $u_0 = \frac{\mathrm{Ku}\cdot\eta}{\tau}$, box volume L^2, $dt = 0.0005$, 5000 time steps after an initial transient of $\frac{100}{dt}$ time steps.

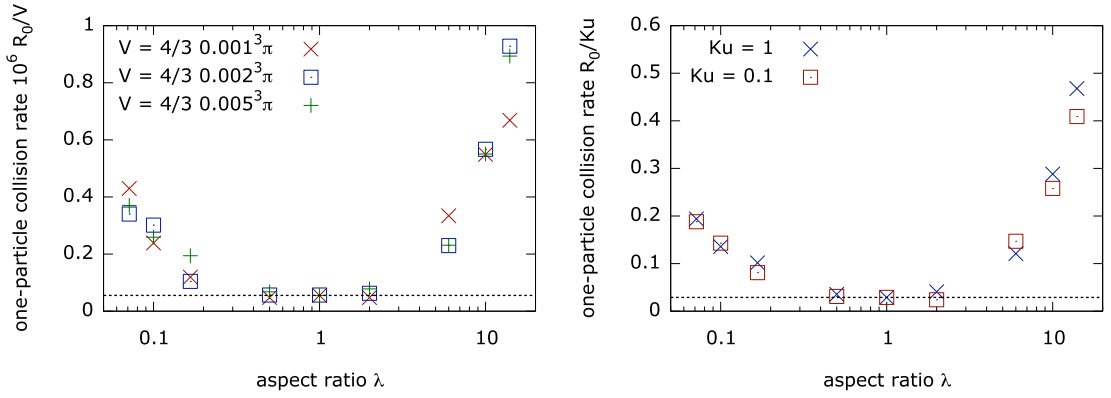

(a) **(b)**

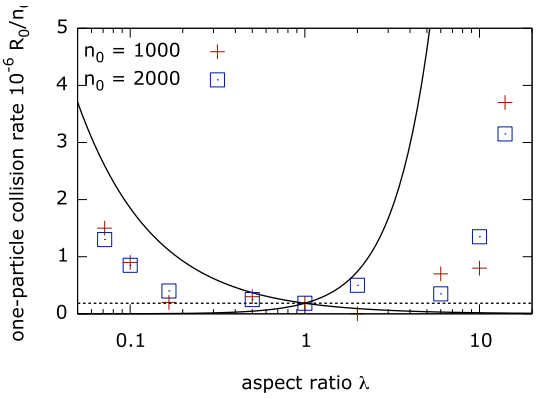

(c)

Figure 7.2: One particle collision rate for three-dimensional spheroidal particles with aspect ratio λ in the random flow. Random initialization of positions and angles. Markers represent only 1 independent experiment. The black lines illustrate the curves for the corresponding spherical particles with radius $a = \left(\frac{3V}{4\lambda\pi}\right)^{\frac{1}{3}}$ and λa according to (3.9). The dashed lines emphasize the value for $\lambda = 1$. (a) Effect of the particle volume V, $L = 0.5$, Ku$= 1$, $n_0 = 1000$. (b) Effect of the Kubo number, $L = 0.5$, $V = \frac{4}{3}0.005^3\pi$, $n_0 = 1000$. (c) Effect of the particle number density n_0, $L = 0.5$, $V = \frac{4}{3}0.002^3\pi$, Ku $= 0.1$. Further simulation parameters: $\eta = 0.1$, $\tau = 0.1$, $u_0 = \frac{\text{Ku}\cdot\eta}{\tau}$, box volume L^3, $dt = 0.0005$, 5000 time steps after an initial transient of $\frac{100}{dt}$ time steps.

8

Conclusion and future ideas

In the thesis the collision rate of axi-symmetric particles in several fluid flows was discussed as a continuation of work that has been done on spherical particles and it was observed that the shape of the particles has a tremendous impact on the collision rate. In particular, particles in the kinetic limit, the shear flow and the random flow model were investigated.

In two spatial dimensions an ansatz of a theoretical collision rate was presented. The collision rate depends on the surfaces that are drawn by the centres of two touching ellipses. It was found that the curves have the same length no matter which relative angle the ellipses have, which affects and simplifies the collision rate as well. The surfaces were not investigated in three dimensions, however the simulations indicate that the surfaces do no longer have the same area.

It was seen that the collision rate for particles that have a random velocity, both translational and rotational, results in the collision rate that is known from kinetic gas theory. It was seen that changing the shape factor Λ to a non-vanishing value while keeping the particle volume constant leads in general to an increase of the collision rate. Due to symmetries in the system (isotropy) the rotation rate is not influencing the collision rate.
The shear flow, which is a laminar and deterministic flow, could be solved for advected ($\mathrm{St} = 0$) particles. Even though there are still unexplained deviations from the theory, progress was made in understanding the behaviour of those particles. In two dimension the collision rate is expected to approach zero, as particles tend to be aligned with the flow the longer they are. In three dimension it was seen that this is not the case anymore. The three dimensional Jeffery orbits give rise to much more collisions. Moreover it was found that the initial configuration of the particles is determining the collision rate.
The most interesting example is the random flow, imitating the small scales of turbulence. Increasing the shape factor $|\Lambda|$ results in a higher collision rate, even though in two dimensions it first drops a bit. It was concluded that several mechanisms, like fluctuations but also the bigger collision radius of more elongated particles, can reason the behaviour.
In order to verify the simulations further, it would be necessary to investigate easier cases where it is also possible to solve the integrals. However, one also has to note that the numerical solution of the integral, that was done by Mathematica, is not exact and can contain errors. Moreover it is not possible at this point to compare to any theory in three dimensions.

Therefore future steps could be to find a parametrization of the surfaces drawn by the centres of touching spheroids, as this turned out to be even more complicated. Nevertheless it would be an interesting task because in the end it would give rise to the theoretical expression for the collision rate in three dimensions. The ansatz would be very similar to the way it was presented in my work.
One could also think about transforming one spheroid into a sphere and investigate the collision between those two bodies which would obviously be much easier. It is not assured that this transformation fulfills all requirements, i.e. that the second spheroid actually stays a spheroid not deforming in a strange way, such that one can easily check for collisions. It would be a very elegant way of dealing with the problem. A two dimensional attempt was previously given in [30].
Likewise inertial particles could be considered. The Jeffery equations for weakly inertial particles was already found in [6], so it would be straight forward to investigate this using the results of this thesis.
Also, while introducing the Navier-Stokes equation in chapter 2 additional external forces were neglected. They can basically be everything, but gravitational forces seem to be the most natural choice to begin with. The particles will not only move according to the flow but at the same time they will settle.
Further on the results from the random flow could be compared to real turbulence data obtained by direct numerical simulations in order to see if the they coincide. This corresponds precisely to the case that was discarded from the beginning, i.e. resolving the flow by finding (numerical) solutions to the Navier-Stokes equations. To find a theoretical expression however is a rather tough task to solve in both cases.

In conclusion, the work done within this project investigates the problem from a fundamental point of view and can be used to approach more physical situations by including more realistic assumptions both from a theoretical but also from a computational perspective.

Bibliography

[1] J. Abrahamson. *Collision rates of small particles in a vigorously turbulent fluid.* Chemical Engineering Science, 30:1371–1379, 1975.

[2] H. Beuther, R. S. Klessen, C. P. Dullemond, and T. Henning. *Protostars and Planets VI.* University of Arizona Press, 2014.

[3] E. Bodenschatz, S. P. Malinowski, R. A. Shaw, and F. Stratmann. *Can We Understand Clouds Without Turbulence?* Science, 327:970–971, 2010.

[4] P. M. Cohn. *Basic Algebra: Groups, Rings and Fields.* Springer, 2003.

[5] L. Davidson. *Fluid Mechanics, Turbulent Flow and Turbulence Modeling.* Lecture Notes, 2016.

[6] J. Einarsson. *Orientational Dynamics of Small Non-Spherical Particles in Fluid Flows.* Licentiate thesis, University of Gothenburg, Department of Physics, 2013.

[7] J. Einarsson. *Angular Dynamics of Small Particles in Fluids.* PhD thesis, University of Gothenburg, Department of Physics, 2015.

[8] G. Falkovich, A. Fouxon, and M. G. Stepanov. *Acceleration of rain initiation by cloud turbulence.* Nature, 419(6903):151–154, 2002.

[9] J. Guasto, R. Rusconi, and R. Stocker. *Fluid mechanics of planktonic microorganisms.* Annual Review of Fluid Mechanics, 44(1):373–400, 2012.

[10] K. Gustavsson. *Advective Collisions in Random Flows.* Licentiate thesis, University of Gothenburg, Department of Physics, 2009.

[11] K. Gustavsson. *Inertial Collisions in Random Flows.* PhD thesis, University of Gothenburg, Department of Physics, 2011.

[12] K. Gustavsson and B. Mehlig. *Statistical Models for Spatial Patterns of Heavy Particles in Turbulence.* Advances in Physics, 65:1–57, 2016.

[13] G. B. Jeffery. *The Motion of Ellipsoidal Particles Immersed in a Viscous Fluid.* The Royal Society, 102(715):161–179, 1922.

[14] A. N. Kolmogorov. *The local structure of turbulence in incompressible viscous fluid for very large Reynolds numbers.* Proceedings of the USSR Academy of Sciences, 30:299–303, 1941.

[15] J. McDonough. *Lectures in Elementary Fluid Dynamics.* Lecture Notes, 2009.

[16] T. Nishikawa, Z. Toroczkai, and C. Grebogi. *Advective coalescence in chaotic flows*. Physical Review Letter, 87(038301), 2001.

[17] A. Pumir. *Private communication*. 2016.

[18] P. Saffman and J. Turner. *On the collision of drops in turbulent clouds*. Journal of Fluid Mechanics, 1:16–30, 1956.

[19] C. Sanderson and R. Curtin. *Armadillo: a template-based C++ Library for Linear Algebra*. Journal of Open Source Software, 1:26, 2016.

[20] R. A. Shaw. *Particle-turbulence interactions in atmospheric clouds*. Annual Review of Fluid Mechanics, 35:138–227, 2003.

[21] M. Smoluchowski. *Versuch einer mathematischen Theorie der Koagulationskinetik kolloider Lösungen*. Zeitschrift für physikalische Chemie, 92:129–168, 1917.

[22] P. Terdiman. *Sweep-and-prune*, 2007.

[23] D. Tritton. *Physical Fluid Dynamics*. Oxford Science Publ. Clarendon Press, 1988.

[24] F. C. van den Bosch. *Physical Processes in Astronomy*. Lecture Notes, 2016.

[25] N. van Kampen. *Stochastic Processes in Physics and Chemistry*. Elsevier, 1992.

[26] W. Wang, J. Wang, and M.-S. Kim. *An algebraic condition for the separation of two ellipsoids*. Computer Aided Geometric Design, 18:531–539, 2001.

[27] W. Wang, M.-S. Kim, Y.-K. Choi, J.-W. Chang, and G. Elber. *Continuous Collision Detection for Ellipsoids*. IEEE Transactions on Visualization & Computer Graphics, 15:311–325, 2008.

[28] M. Wilkinson, B. Mehlig, and V. Bezuglyy. *Caustic Activation of Rain Showers*. Physical review letters, 97, 2006.

[29] M. Wilkinson, B. Mehlig, and V. Uski. *Stokes trapping and planet formation*. The Astrophysical Journal Supplement Series, 176:484–496, 2008.

[30] X. Zheng and P. Palffy-Muhoray. *Distance of closest approach of two arbitrary hard ellipses in two dimensions*. Phys. Rev. E, 75:061709, 2007.

A

Statistical model of turbulence

Solving the Navier-Stokes equation for turbulence can be tedious work to do in order to get the underlying flow field. The parameter space is immense, the equations are non-linear and therefore the computer power needed exceeds today's resources in many cases.
For that reason it has become a successful method to approximate turbulence by a random flow field instead. The model is such that it has the same statistical properties, e.g. the flow speed u_0, the correlation length η, the correlation time τ, as the actual turbulence. The beauty with it is that it can be easily implemented and it was shown in many comparisons to direct numerical simulations that the results are qualitatively the same and help us to understand basic mechanisms.
The topic of the last part of the thesis is finding the collision rate of spheroids in an incompressible random flow. Thus it is essential to say some words about how to generate it. In [10] a detailed description is given but the important aspects are summarized in the following.

A.1 Creation of a random velocity field

The model in d dimensions is based on time-dependent random Gaussian functions of form

$$\Psi(\mathbf{r},t) = (2\pi)^{d/4}\frac{\eta^{d/2+1}u_0}{\sqrt{V_d d(d-1)}}\sum_{\mathbf{k}} a_{\mathbf{k}}(t)\exp\left[\mathrm{i}\mathbf{k}\cdot\mathbf{r} - \frac{k^2\eta^2}{4}\right]. \tag{A.1}$$

In two dimensions $\mathbf{k} = 2\pi\left(\frac{n_x}{L_x}, \frac{n_y}{L_y}\right)^T$, $n \in \mathbb{Z}$. The box volume $V_2 = L_xL_y$ is characterized by its side lengths L_x and L_y. In other dimensions these variables are analogous.
Ψ is a Fourier series and the Fourier coefficients $a_{\mathbf{k}}(t)$ are complex Gaussian random numbers with properties

$$\begin{aligned}\langle a_{\mathbf{k}}(t)\rangle &= 0\\ \langle a_{\mathbf{k}}(t)a^*_{\mathbf{k}},(t)\rangle &= \delta_{\mathbf{k}\mathbf{k}},\\ a^*_{\mathbf{k}}(t) &= a_{\text{-}\mathbf{k}}(t).\end{aligned}$$

The last conditions results in (A.1) being real which is absolutely crucial.

In order to update the function in time only the coefficients are updated using another set of complex Gaussian random numbers $b_{\mathbf{k}}$.

$$\begin{aligned}\langle b_{\mathbf{k}}(t)\rangle &= 0\\ \langle b_{\mathbf{k}}(t)b^*_{\mathbf{k}},(t)\rangle &= \left(1-\exp\left[-\frac{\delta t}{\tau}\right]\right)\delta_{\mathbf{kk}'} \approx \frac{2\delta t}{\tau}\delta_{\mathbf{kk}'}.\end{aligned}$$

Finally the update rule is

$$a_{\mathbf{k}}(t+\delta t) = \exp\left[-\frac{\delta t}{\tau}\right]a_{\mathbf{k}}(t) + b_{\mathbf{k}} \approx (1-\frac{\delta t}{\tau})a_{\mathbf{k}}(t) + b_{\mathbf{k}}.$$

All this results in $\langle\Psi(\mathbf{r},t)\rangle = 0$ and a correlation function

$$\begin{aligned}\langle\Psi(\mathbf{r},t)\Psi(\mathbf{r}',t')\rangle &= \frac{\eta^2u_0^2}{d(d-1)}\exp\left[-\frac{(\mathbf{r}-\mathbf{r}')^2}{2\eta^2}-\frac{|t-t'|}{\tau}\right]\\ &= \frac{\eta^2u_0^2}{d(d-1)}\exp\left[-\frac{R^2}{2\eta^2}-\frac{T}{\tau}\right]\equiv\mathcal{C}(R,T),\end{aligned}$$

if the correlation length η is small compared to the system size L_i. Figure A.1 shows the importance of the condition $\eta \ll L_i$, as if the condition is not fulfilled the correlations of the Gaussian function and its derivatives deviate. For $\eta = 0.1$ $L_i \geq 1$ would be a good choice. If $L_i = 0.5$ the correlations are reproduced well only on the small scale, and by further decreasing the box length, e.g. $L_i = 0.25$, the correlations are getting completely wrong.
The prefactor of the random function is chosen such that $\langle\mathbf{u}(\mathbf{r},t)\mathbf{u}(\mathbf{r},t)\rangle = u_0^2$ which represents the characteristic flow speed. If this had not been the case, one would have had to take care of the right normalization. Eventually the velocity field $\mathbf{u}(\mathbf{r},t)$ and its gradient $\mathbb{A}(\mathbf{r},t)$ of the random flow in two and three dimensions is constructed as follows.

$$\begin{aligned}\textbf{2d}: \quad \mathbf{u}(\mathbf{r},t) &= \begin{pmatrix}\partial_y\Psi\\ -\partial_x\Psi\end{pmatrix}\\ \mathbb{A}(\mathbf{r},t) &= \nabla\mathbf{u}^T(\mathbf{r},t) = \begin{pmatrix}\partial_x\partial_y\Psi & -\partial_x^2\Psi\\ \partial_y^2\Psi & -\partial_y\partial_x\Psi\end{pmatrix}\\ \textbf{3d}: \quad \mathbf{u}(\mathbf{r},t) &= \nabla\times\mathbf{\Psi} = \begin{pmatrix}\partial_x\\ \partial_y\\ \partial_z\end{pmatrix}\times\begin{pmatrix}\Psi_1\\ \Psi_2\\ \Psi_3\end{pmatrix} = \begin{pmatrix}\partial_y\Psi_3-\partial_z\Psi_2\\ -\partial_x\Psi_3+\partial_z\Psi_1\\ \partial_x\Psi_2-\partial_y\Psi_1\end{pmatrix}\\ \mathbb{A}(\mathbf{r},t) &= \nabla\mathbf{u}^T(\mathbf{r},t) = \begin{pmatrix}\partial_x(\partial_y\Psi_3-\partial_z\Psi_2) & \partial_x(-\partial_x\Psi_3+\partial_z\Psi_1) & \partial_x(\partial_x\Psi_2-\partial_y\Psi_1)\\ \partial_y(\partial_y\Psi_3-\partial_z\Psi_2) & \partial_y(-\partial_x\Psi_3+\partial_z\Psi_1) & \partial_y(\partial_x\Psi_2-\partial_y\Psi_1)\\ \partial_z(\partial_y\Psi_3-\partial_z\Psi_2) & \partial_z(-\partial_x\Psi_3+\partial_z\Psi_1) & \partial_z(\partial_x\Psi_2-\partial_y\Psi_1)\end{pmatrix}.\end{aligned}$$

$\mathbf{\Psi} = (\Psi_1,\Psi_2,\Psi_3)^T$ consists of three independent (i.e. $\langle\Psi_m(\mathbf{r},t)\Psi_n(\mathbf{r}',t')\rangle = \delta_{mn}C(R,T)$) random Gaussian functions of the previously described type. Obviously $Tr(\mathbb{A}) = 0$. This is an equivalent statement to $\nabla\cdot\mathbf{u}(\mathbf{r},t) = 0$ which confirms the incompressibility of the flow.

The correlation functions of the components of $\mathbf{u}$ and respectively $\mathbb{A}$ are in two and three spatial dimensions then given by

$$\begin{aligned}\langle u_i(\mathbf{r},t)u_j(\mathbf{r}',t')\rangle &= (-\delta_{ij}(\Delta-\partial_i^2)+(1-\delta_{ij})\partial_i\partial_j)\ \mathcal{C}(R,T)\\ &= \left[-\delta_{ij}\left(-\frac{d-1}{\eta^2}+\frac{R^2-(r_i-r_i')^2}{\eta^4}\right)\right.\\ &\quad \left.+(1-\delta_{ij})\frac{(r_i-r_i')(r_j-r_j')}{\eta^4}\right]\mathcal{C}(R,T)\end{aligned}$$

$$\begin{aligned}\langle \mathbb{A}_{ij}(\mathbf{r},t)\mathbb{A}_{kl}(\mathbf{r}',t')\rangle &= \langle \partial_j u_i(\mathbf{r},t)\partial_l u_k(\mathbf{r}',t')\rangle\\ &= (-1)^{\delta_{jl}}\partial_j\partial_l\ \langle u_i(\mathbf{r},t)u_k(\mathbf{r}',t')\rangle.\end{aligned}$$

δ_{ij} is the Kronecker-Delta and $i,j,k,l \in x,y,z$ and ∂_i the partial derivative with respect to i. $\Delta=\nabla^2$ is the Laplace operator.
In particular,

$$\begin{aligned}\langle \mathbb{A}_{xx}(\mathbf{r},t)\mathbb{A}_{xx}(\mathbf{r}',t')\rangle &= \partial_x^2(\Delta-\partial_x^2)\,\mathcal{C}(R,T)\\ &= \frac{(\eta^2-(r_x-r_x')^2)\left[(d-1)\eta^2-(R^2-(r_x-r_x')^2)\right]}{\eta^8}\,\mathcal{C}(R,T)\end{aligned} \tag{A.2}$$

$$\langle \mathbb{A}_{xx}(0,0)\mathbb{A}_{xx}(0,0)\rangle = \frac{u_0^2}{d\cdot\eta^2}. \tag{A.3}$$

With this it was presented how to generate a random incompressible flow with a velocity field $\mathbf{u}(\mathbf{r},t)$ and velocity gradients $\mathbb{A}(\mathbf{r},t)$ which obeys the properties of a turbulent flow with characteristic flow speed u_0, correlation length η, correlation time τ and Kubo number $Ku=\frac{u_0\tau}{\eta}$.

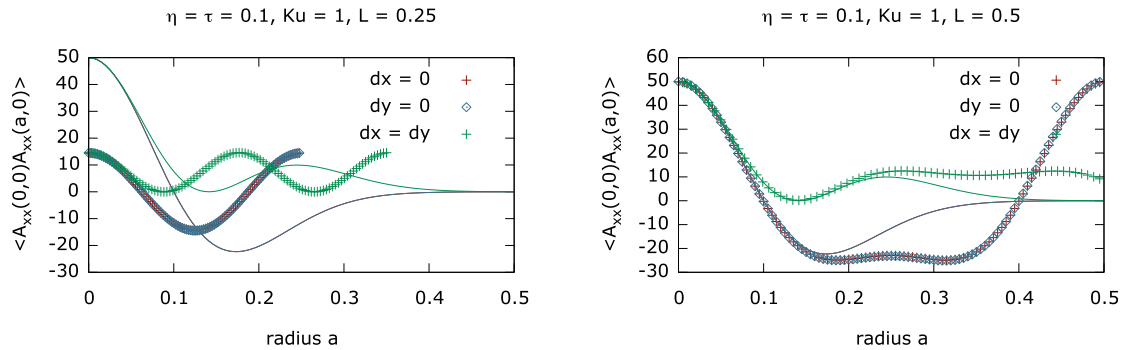

(a) **(b)**

Figure A.1: Correlation function $\langle A_{xx}(0,0)A_{xx}(\mathbf{r},0)\rangle$ in two dimensions for two different boxes with length $L=0.25$ (a) and $L=0.5$ (b) in each dimension. Three different constraints on the distance $\mathbf{r}$, i.e. on $dx=r_x-r_x'$ and $dy=r_y-r_y'$. Markers represent the mean of 300000 independent experiments with each 100 particles. The error is significantly small. Lines show the theory from (A.2). Parameters: Ku = 1, $\eta=\tau=0.1$.

A.2 Optimisation

Besides the theoretical concept of a random flow it is also important to think about a reasonable implementation of it. For this reason the upcoming part shows further practical simplifications of (A.1) used in the simulations.

In the implementation of the flow depending on a Gaussian random function as (A.1) the equation was further optimised in order to avoid complex numbers and gain computation speed. The main idea is to rewrite the sum. The basic property that allows this is $a^*_{\mathbf{k}}(t) = a_{\text{-}\mathbf{k}}(t)$. To make the calculation more clearly $\mathbf{k} \equiv (m,n)^T$ and $a_{\mathbf{k}}(t) \equiv a_{mn}$ is used.

$$\begin{aligned}
&\sum_{\mathbf{k}} a_{\mathbf{k}}(t) \exp\left[\mathrm{i}\mathbf{k}\cdot\mathbf{r} - \frac{k^2\eta^2}{4}\right] \\
&\quad= \sum_{m,n=-\infty}^{\infty} a_{mn} \exp\left[\mathrm{i}(mx+ny) - \frac{(m^2+n^2)\eta^2}{4}\right] \\
&\quad= a_{00} + \sum_{m\neq 0} a_{m0} \exp\left[\mathrm{i}mx - \frac{m^2\eta^2}{4}\right] + \sum_{n\neq 0} a_{0n} \exp\left[\mathrm{i}ny - \frac{n^2\eta^2}{4}\right] \\
&\qquad+ \sum_{m,n\neq 0} a_{mn} \exp\left[\mathrm{i}(mx+ny) - \frac{(m^2+n^2)\eta^2}{4}\right]
\end{aligned}$$

The individual sums can be simplified further. It is shown for only one case. However, the principles are exactly the same for all other sums.

$$\begin{aligned}
&\sum_{m\neq 0} a_{m0} \exp\left[\mathrm{i}mx - \frac{m^2\eta^2}{4}\right] \\
&\quad= \sum_{m>0} \left(a_{m0}\exp\left[\mathrm{i}mx\right] + a_{-m0}\exp\left[-\mathrm{i}mx\right]\right) \exp\left[-\frac{m^2\eta^2}{4}\right] \\
&\quad= \sum_{m>0} \left(a_{m0}\exp\left[\mathrm{i}mx\right] + a^*_{m0}\exp\left[-\mathrm{i}mx\right]\right) \exp\left[-\frac{m^2\eta^2}{4}\right] \\
&\quad= \sum_{m>0} \left((a_{m0}+a^*_{m0})\cos\left[mx\right] + \mathrm{i}(a_{m0}-a^*_{m0})\sin\left[mx\right]\right) \exp\left[-\frac{m^2\eta^2}{4}\right] \\
&\quad= \frac{2}{\sqrt{2}} \sum_{m>0} \left(\Re(a_{m0})\cos\left[mx\right] - \Im(a_{m0})\sin\left[mx\right]\right) \exp\left[-\frac{m^2\eta^2}{4}\right]
\end{aligned}$$

considering Euler's formula and that both the real and imaginary part of a_{mn} are real Gaussian random numbers having the same mean and variance as a_{mn}. This leads to an additional factor of $\frac{1}{\sqrt{2}}$.

Using the same trick for all sums the two dimensional $\Phi(\mathbf{r}, t)$ becomes

$$\begin{aligned}\Phi(\mathbf{r},t) \propto\ a_{00} + \Bigg[& \frac{2}{\sqrt{2}} \sum_{m,n>0} \left(\Re(a_{m0})\cos[mx] - \Im(a_{m0})\sin[mx]\right) \exp\left[-\frac{m^2\eta^2}{4}\right] \delta_{n,\frac{2\pi}{L_y}} \\ & + \left(\Re(a_{0n})\cos[ny] - \Im(a_{0n})\sin[ny]\right) \exp\left[-\frac{n^2\eta^2}{4}\right] \delta_{m,\frac{2\pi}{L_x}} \\ & + \Big(\Re(a_{mn})\cos[mx+ny] - \Im(a_{mn})\sin[mx+ny] \\ & + \Re(a_{m-n})\cos[mx-ny] - \Im(a_{m-n})\sin[mx-ny]\Big) \exp\left[-\frac{(m^2+n^2)\eta^2}{4}\right]\Bigg].\end{aligned}$$

Merging everything together to one sum there arise two delta functions in order to avoid multiple counting of the sums where one index vanishes.
This sum is theoretically still up to infinity. Indeed it is possible to find criteria where to stop the sum in each dimension of k in order to get a certain precision p. The summands decay exponentially with k ergo the sum converges to a value. For instance, the threshold for m is given here. Again the procedure is the same in the other dimensions.

$$\exp\left[-\frac{m^2\eta^2}{4}\right] \leq 10^{-p} \quad \Leftrightarrow \quad \frac{m^2\eta^2}{4} \geq p \quad \Leftrightarrow \quad m \geq \frac{2\sqrt{p}}{\eta}$$

Summands with m bigger than this value do not contribute within precision p. Equivalently holds

$$m = \frac{2\pi}{L_x} n_x \geq \frac{2\sqrt{p}}{\eta} \quad \Leftrightarrow \quad n_x \geq \frac{L_x}{\pi\eta}\sqrt{p}. \tag{A.4}$$

With this one can control the number of Fourier modes that are taken into account in the evaluation of the flow. But note that while $\frac{L_i}{\eta}$ decreases (i.e. less Fourier modes are used) the statistical model successively loses qualitative properties that are very important in order to imitate turbulence.